Direct introduction MALDI FTICR MS based on dried droplet deposition applied to non-targeted metabolomics on Pisum Sativum root exudates

Valentina Calabrese, Isabelle Schmitz-Afonso, Wassila Riah-Anglet, Isabelle Trinsoutrot-Gattin, Barbara Pawlak, Carlos Afonso

Direct Introduction MALDI FTICR MS based on dried droplet deposition applied to non-targeted metabolomics on *Pisum Sativum* Root Exudates

Valentina Calabrese [a], Isabelle Schmitz-Afonso [a,*], Wassila Riah-Anglet [b], Isabelle Trinsoutrot-Gattin [b], Barbara Pawlak [c], Carlos Afonso [a]

[a] Normandie Univ, COBRA, UMR 6014 and FR 3038, Université de Rouen, INSA de Rouen, CNRS, IRCOF, 1 rue Tesnières, 76821 Mont-Saint-Aignan, Cedex, France.

[b] UniLaSalle, AGHYLE Research Unit UP 2018.C101, Rouen Team, 76134 Mont-Saint Aignan, SFR Normandie Végétal FED 4277, 76000 Rouen, France.

[c] Laboratoire GlycoMEV UR 4358, Université de Rouen Normandie, SFR Normandie Végétal FED 4277, 76000 Rouen, France

*Corresponding author at : Normandie Univ, COBRA, UMR 6014 and FR 3038, Université de Rouen, INSA de Rouen, CNRS, IRCOF, 1 rue Tesnières, 76821 Mont-Saint-Aignan, Cedex, France. E-mail address : isabelle.schmitz-afonso@univ-rouen.fr

Key words Root exudates, Non-targeted metabolomics, Fourier Transform Ion Cyclotron Resonance Mass Spectrometry, MALDI, *Pisum sativum*

Graphical abstract

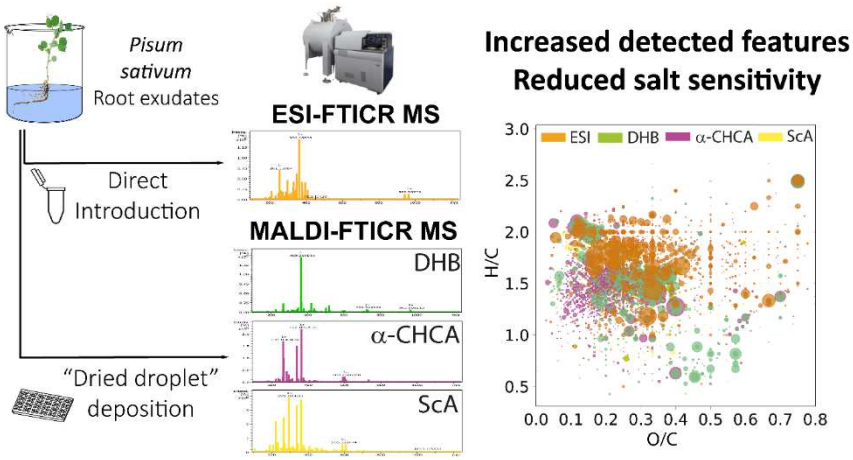

Abstract

Non-targeted metabolomic approaches based on direct introduction (DI) through a soft ionization source are nowadays used for large-scale analysis and wide cover-up of metabolites in complex matrices. When coupled with ultra-high-resolution Fourier-Transform ion cyclotron resonance (FTICR MS), DI is generally performed through electrospray (ESI), which, despite the great analytical throughput, can suffer of matrix effects due to residual salts or charge competitors. In alternative, matrix assisted laser desorption ionization (MALDI) coupled with FTICR MS offers relatively high salt tolerance but it is mainly used for imaging of small molecule within biological tissues. In this study, we report a systematic evaluation on the performance of direct introduction ESI and MALDI coupled with FTICR MS applied to the analysis of root exudates (RE), a complex mixture of metabolites released from plant root tips and containing a relatively high salt concentration. Classic dried droplet deposition followed by screening of best matrices and ratio allowed the selection of high ranked conditions for non-targeted metabolomics on RE. Optimization of MALDI parameters led to improved reproducibility and precision. A RE desalted sample was used for comparison on ionization efficiency of the two sources and ion enhancement at high salinity was highlighted in MALDI by spiking desalted solution with inorganic salts. Application of a true lyophilized RE sample exhibited the complementarity of the two sources and the ability of MALDI in the detection of undisclosed metabolites suffering of matrix effects in ESI mode.

1. Introduction

Non-targeted metabolomics is a growing field of 'omics' which enables the unbiased detection and annotation of a wide range of molecules at low molecular weight (< 1500 Da) in biological samples [1–6]. In the case of plant science, metabolite profiling could give access to the characterization of primary and secondary metabolites which are widely involved in plant growth, development and health or adaptation to abiotic and biotic stress. It could be drought, extremes temperatures, salinity or attack by pathogenic microorganisms [7–13]. Non-targeted metabolomic is typically performed through nuclear magnetic resonance (NMR) [14,15] and mass spectrometry (MS) [16]. Over the past decades, MS coupled with gas (GC-MS) [17] or liquid chromatography (LC-MS) [18] has been widely used as preferred technique for the detection of a wide range of compounds in plant material. In the case of complex matrices, LC-MS allows the separation of isomeric and isobaric species before their

detection as ions in gas-phase [19]. Chromatographic separation allows a reduction of sample complexity but it is a highly time-consuming technique and it presents some limitations in large-scale non-targeted metabolomic studies [20]. Recently, non-targeted metabolomic approaches based on the direct introduction (DI) of the sample into the ion source have been proved to enable faster analysis for large-scale study and wide cover-up of metabolite detection [21,22]. Among these, direct introduction coupled with ultra-high-resolution analyzers as in Fourier Transform ion cyclotron resonance mass spectrometry (FTICR MS) [23,24] has been increasingly used in non-targeted metabolomic thanks to its advantages in ultra-high resolving power, high mass accuracy and dynamic range [25–28]. Recently, many studies have been published on the potentiality of FTICR MS to perform a global profiling of metabolites in plants material [27–31]. FTICR analyzers enable separation according to the cyclotron frequency produced by the rotation of ions in a fixed magnetic field and the simultaneous detection of all *m/z* over a time range [32]. In this extent, when coupled with FTICR MS, direct introduction allows to obtain a constant number of ions entering into the ICR cell during wide time ranges, leading to ultra-high resolution and mass measure precision. For this reason, direct introduction FTICR MS is normally preferred over hyphenation with liquid chromatography. Direct introduction FTICR MS coupled with electrospray (ESI) is routinely used as preferred source in non-targeted metabolomic studies because it enables the easy and efficient ionization of a wide range of metabolites characterizing many biological matrices [33–35]. However, ESI suffers from some analytical limitations as matrix effects [36]. In fact, when a wide number of different analytes is injected in the source, ions might compete as charge carriers (ion competition) or species at high abundance can lead to reduced sensitivity of low abundance ones (ion suppression) [37–39].

Matrix assisted laser desorption ionization (MALDI) is an alternative ion source which enables the soft ionization of a wide range of metabolites in biological samples [40]. This is normally performed through the use of an organic matrix which assists the transfer of the laser energy to the analyte, enabling the ionization and reducing ion fragmentation. MALDI enables the performant detection of metabolites in complex biological samples without preliminary clean-up or separation before analysis. However, when coupled with classical mass analyzers such as time of flights, the presence of matrix ions in the low *m/z* zone limits its applications in the analysis of low molecular weight compounds [41]. MALDI has therefore been applied mostly in the analysis of large organic biomolecules such as lipids and proteins[42,43], peptides [44,45] and saccharides [46] or in whole-cell samples analysis for the detection of intact microorganisms [47]. Lately, coupling with FTICR MS has boosted

application of MALDI in low molecular weight compounds discovery thanks to improved molecular formula assignment for isobaric ions [48,49]. Nonetheless, MALDI-FTICR MS is nowadays mainly used in metabolomics to highlight the spatial distribution of a reduced number of compounds within biological tissues [50,51]. Many studies point out on imaging for biomedical applications or in plant science [52–58]. Nonetheless, to the best of our knowledge, few studies points out on a non-targeted metabolomic approach based on the direct introduction of a biological sample based on MALDI-FTICR MS [59]. In fact, the highest drawback of mass spectrometry based on MALDI is that, besides from problems connected to the noise in the low mass region [60], ionization depends strictly on the homogeneity of the matrix-sample spot [61]. This can lead to issues as lack of reproducibility for qualitative and mostly quantitative analysis [62].

In this study we present for the first time an analytical optimization of a non-targeted metabolomic approach based on ultra-high-resolution mass spectrometry coupled to direct introduction MALDI for improved metabolite detection and reduced ion suppression in presence of salts. This method has been optimized on plant root exudates (RE), because this complex biological cocktail contains a high number and diversity of molecules and residual salts [11]. Indeed, RE is a mixture of primary and secondary metabolites produced by the plant roots and continuously released into the narrow zone of soil surrounding roots called the rhizosphere [12]. These include many compounds of different nature which take a large part in the interactions between plants and their environment [63,64], especially with the rhizosphere microbiota essential to plant growth, health and resistance to biotic or abiotic stress [12,64–67]. Deciphering molecular signals exchanged between the root and its microbiota would be an important advancement in plant science and a great hope for agroecology, because a better control of interactions in the rhizosphere could allow limitation of phytochemical inputs in agricultural processes [68]. These objectives could be reached through the metabolomic investigation and profiling of plant RE [11,69]. Nonetheless, due to the complexity of RE composition and its variability with plant growth conditions and variety, performing metabolomic studies of root exudates is challenging and many efforts are required for the optimization of both RE collection [70] and analysis through mass spectrometry techniques [71]. RE sampling is usually divided in two steps consisting in plant growth and metabolite extraction [72]. Among many plant growth methods, artificial hydroponic systems are widely used as they enable an easier handling of plants and improved reproducibility with low root damage and reduced metabolites absorption from matrix [70,73]. In hydroponics, plant growth is obtained through immersion of seeds and roots in a nutritive medium

containing macronutrient [74]. Once growth completed, RE can be collected by rinsing, then transferring the root system from the hydroponic medium to a solvent that is compatible with analysis (i.e. water) [75,76]. It is worth to note that, in RE samples obtained from hydroponic systems, metabolites occur at mM–nM concentrations; while a relatively high concentration of macronutrients (mM) may be present after re-concentration of RE samples [77]. Therefore, in the case of mass spectrometry-based metabolomics coupled with direct introduction, metabolite extraction and salt removal are highly advised to obtain the preferential ionization of the metabolites over suppression and competition effects [71].

Here, we evaluated the performances of MALDI-FTICR MS based on dried droplet deposition to a non-targeted metabolomic approach for the detection and annotation of low abundance metabolites in *Pisum sativum* RE. Literature presents many studies on *P. sativum* RE showing the presence of amino acids, sugars and organic acids [78], while few investigations focus on the isolation and characterization of secondary metabolites. The main chemical classes have been found to be triterpenes [79], polyphenols [80,81], alkaloids [82] and some classes of specialized phytohormones [83–85]. Nonetheless, to the best of our knowledge, this is the first non-targeted metabolomic study on *P. sativum RE*. In this study, a *P. sativum* RE desalted sample was first submitted to a classic non-targeted metabolomic approach based on data dependent acquisition mass spectrometry (DDA-MS) and to ESI-FTICR MS. A collection of 48 metabolites were annotated with a hypothetical structure and a global profiling with an insight of different chemical classes was obtained *via* unique molecular formula assignment. This information was used for the main aim of this study, which attempted a development of a non-targeted metabolomic approach based on MALDI-FTICR MS. A screening on the performances of six MALDI matrices and 36 different conditions (sample/matrix ratio, with or without addition of acid) led to the selection of three optimal combinations which enabled a satisfying non-targeted metabolite detection. Moreover, a rigorous control of experimental parameters such as the laser power used for MALDI measurements enabled an improvement of mass accuracy without complex sample deposition, which was based on the dried droplet method. MALDI resulted a complementary technique, leading to a ~60% increase of detected metabolites at both low and at high *m/z* values. Matrix effects arising from increased salinity in ESI-FTICR MS and MALDI-FTICR MS mode were evaluated on desalted *P. sativum* RE samples which were spiked with increasing amounts of salts. Lastly, the optimized non-targeted metabolomic approach based

on MALDI was tested on a true lyophilized *P. sativum* RE sample containing a natural amount of salt arising from the exudation step.

2. Material and methods

2.1 Collection of plant root exudates.

Plant seeds were purchased from RAGT Semences (Toulouse, France). Seeds were cleaned and stored in containers at 5 °C in a cool room until use. Pea seeds were soaked twice for 10 min in an ethanol solution (96%) and then in a hypochlorite solution (26 %) under stirring. After each immersion, the seeds were rinsed six times with demineralized sterile water (10 s per rinse). The disinfection process was carried out in sterile conditions. For germination, sterilized seeds of pea were cultivated in boxes with agar (1 %). The seeds were germinated in phytotronic chamber at a day/night cycle: 16 h, 23 °C / 8 h, 20 °C for a period of 7 days. After germination, seed were transferred in a hydroponic system containing ¼ Hoagland nutrient solution and cultured in a phytotronic chamber in the same condition as germination. A list of the oligo and micro elements with their concentration in the ¼ diluted Hoagland solution can be found in table 1S. Five weeks growth seedling characterized of 6-8 leaves each plant were used for exudation. Briefly, the plants roots were removed from the Hoagland solution and briefly rinsed with sterile deionized water to remove the remaining nutrient solution. The plants were then transferred to backers containing 500 mL sterile ultrapure water. Exudation was carried out for 1h, roots were then removed and the solutions frozen at -20°C in glass bottles. A blank solution was prepared using 500 mL sterile ultrapure water which was incubated in the similar conditions as backers of root exudates.

2.2 Metabolites extraction.

Two sample treatment methods were used for metabolites extraction and concentration. Desalted sample which contained an enriched fraction of *P. sativum* RE were obtained through solid phase extraction (SPE). Briefly, frozen *P. sativum* RE (500 mL) were completely thawed, distributed in tubes (Falcon) and solutions were centrifugated at low temperature (5°C) for 15 min at 10 000 rpm (Eppendorf 5804 R) in order to remove cell debris and eventual particles. Aliquots of supernatant liquid were collected to reach a final volume of 420 mL. Centrifuged RE solution were then submitted to SPE on an automated SPE WorkStation (6.25ws, Interchim France). A column filled with a hydrophilic modified

styrene-based polymer (PolyClean HLB, 3 mL x 200 mg, Interchim France) was used for the extraction of metabolites. The HLB column was washed prior to sample loading with 5 mL of methanol and 5 mL of water at a flow rate of 15 mL/min. RE were then passed through the activated polymeric cartridge at 3 mL/min. The polymeric phase was washed with 4 mL of LC-MS water at 3 mL/min and dried for 10 min using a gentle stream of nitrogen. Elution was then performed by passing through 3 mL methanol at 2 mL/min. Time spent for SPE extraction was around 3h for sample. The fraction was then dried completely under a nitrogen stream and resuspended in 250 µL of water. Blank was treated likewise. Samples were kept at low temperature (5-7°C) during SPE and evaporation by soaking bottles in ice. This assured minimal degradation of metabolites during the time-consuming sample treatment. For lyophilized samples, sample treatment was similar, except that after centrifugation the final volume of 420 mL RE was distributed in clean tubes, frozen at -20°C for 24h and then lyophilized using a freeze dryer (BUCHI Lyovapor™ L-200). The lyophilized sample and a blank were resuspended both in 250 µL of water. SPE and lyophilized samples were stored at -20°C until analysis.

2.3 Sample preparation and DDA-MS measurements for metabolites annotation.

P. sativum RE SPE extracts were thawed before analysis and solutions were directly submitted to DDA-MS without further treatment. The mass spectrometer was a hybrid quadrupole-time-of-flight instrument (QTOF, Synapt G2 HDMS, Waters MS Technologies, Manchester, UK) [86] coupled with an ultra-high-performance liquid chromatographic (UHPLC) system equipped with a diode array detector (Vanquish, Thermo Scientific, San Jose, CA, USA). The travelling wave ion mobility cell included in the instrument was not used during analysis. The column used for the elution was a reverse phase ACQUITY UPLC HSS T3 1.7 µm of dimension 1.0 mm x 100 mm (Waters Manchester, UK) equipped with a 0.2 µm prefilter. The sample tray and column oven temperatures were set at 8 °C and 50 °C, respectively. The injection volume was set at 5 µL for MS/MS measurements in positive mode and 10 µL in negative mode. Flow rate of 0.100 mL/min was used. Mobile phase A consisted of water + 0.1 % formic acid and mobile phase B of acetonitrile + 0.1 % formic acid. The elution was the following: 0–2 min, 0% B; 2–3 min, 0–10% B; 3–10 min, 10–20% B; 10–14 min, 20–100% B; 14–17 min, 100% B; 17–18 min, 100–0% B; 18–25 min, 0% B. DDA-MS experiments were performed over a *m/z* 50–1200 range in resolution mode (resolution 20 000 FWHM). A sodium formate solution was used for external calibration while a continuous lock mass correction was applied by infusing leucine enkephalin via the

LockSpray™ interface (reference scan frequency 10 sec, lock spray capillary 3.0 kV and cone voltage of 25 V in positive mode and respectively 10 s, 3.0 kV and 50 V in negative mode). Source in positive mode was operated as following: capillary 3 kV, sampling cone 25 V, extraction cone 5 V. The source temperature was 120°C, the cone gas flow and the desolvation gas flows were set respectively to 20 L/h and 600 L/h; desolvation temperature 300 °C. For negative ion mode, parameters were the same excluded for the capillary which was set at 2.2 kV. Metabolites were fragmented automatically through a survey scan function when the precursor threshold peak intensity exceeded 1000 counts in positive mode and 800 scans in negative mode. For each MS scan, the 3 most intense MS/MS ions were fragmented using 4 MS/MS scans accumulation. Then, each fragmented ion was excluded for 6 seconds with a scan time of 0.200 sec and an interscan time of 0.024 sec. Experiments were performed in the transfer cell which was filled with argon (6.10^{-3} mbar), using collision energy ranging from 10-20 eV for low *m/z* values to 10-30 eV for high *m/z* values. A linear variation was used along the whole range. The trap cell of the instrument was operated using a background collision energy of 4 eV.

For metabolites annotation, raw data were submitted to accurate mass measure on MassLynx (v. 4.2, Waters Corporation) and then converted in mzXML open format through the MSConvert tool of ProteoWizard (v. 3.0.9992) using MS1 and MS/MS levels as filters. Raw data were then uploaded on the Global Molecular Networking Platform (GNPS, https://gnps.ucsd.edu) [87,88] and experimental spectra were queried against library search using the spectral library search in order to find possible matches. Ions corresponding to contaminants or matrix were subtracted automatically through the GNPS analysis. Metabolite annotation was performed on manual literature search for some abundant metabolites for which no match was found on GNPS databases.

2.4 Sample preparation and ESI-FTICR MS measurements.

For ESI measurements, 100-fold diluted solutions in water/methanol (50/50, v/v) for both SPE and lyophilized samples were prepared. For measurements in positive ion mode, 0.1 % formic acid was added to the final diluted solution in order to favor protonated forms. Solutions were introduced directly in the electrospray source of a high-field FTICR mass spectrometer (SolariX MRMS, Bruker Bremen, Germany), equipped with a 12 T superconducting magnet and a dynamically harmonized ICR cell, in both positive and negative ion modes. Samples were introduced to the ion source through a syringe pump at a

flow rate of 90.0 µL min^{-1}. Spectra were recorded at a transient length of 1.12 s (4 million points) with an accumulation time of 0.050 s in positive mode and 0.100 s in negative mode. A sodium trifluoroacetate solution at 0.1 mg/mL in acetonitrile/water (50/50, v/v) was used for external calibration by the acquisition of 30 accumulated scan spectra. Mass spectra were acquired over a *m/z* 98−1500 range. A mass resolving power of around 700,000 at *m/z* 200 was achieved. A complete list of parameters used for ESI measurements can be found in Table 2S.

2.5 **Sample preparation for MALDI-FTICR MS measurements**

For MALDI measurements, six matrices were chosen among the most used in MALDI literature. These were: 2,5-Dihydroxybenzoic acid (DHB), alpha-Cyano-4-hydroxycinnamic acid (α-CHCA), Sinapinic acid (ScA), trans-2-[3-(4-tert-Butylphenyl)-2-methyl-2-propenylidene] malononitrile (DCTB), 1,5-Naphthalenediamine (DAN) and 9-Aminoacridine (9-AA). Regarding matrix preparation: DHB and ScA were prepared at a concentration of 10 mg/mL in water/methanol (50/50 v/v) and 9AA at a concentration of 9 mg/mL; α-CHCA at 10 mg/mL in MeOH/ACN (50/50 v/v), DCTB and DAN at 10 mg/mL in MeOH. The same solutions were prepared in duplicate and added of 0.1 % formic acid on the final volume. SPE and lyophilized samples were then mixed without further dilution with the seven matrices with a ratio sample:matrix of 1:1, 2:1 and 1:10. Then, for each mixture, two additional conditions were tested, namely with or without the addition of 0.1 % of formic acid (FA). The dried droplet method was used for sample deposition on a target plate (MTP 384 target plate ground steel BC, Bruker Daltonics, Germany) and for each sample, 5 µL were deposed for each spot, on three different positions and samples gently dried under vacuum. For external calibration in positive mode, a mixture of the 3 peptides bradykinin, leucine enkephalin and angiotensin (each at a concentration of 10 pmol/µL in water) was prepared at a proportion 1:1:1:3 with DHB at 10 mg/mL. In negative ion mode, a solution of 9-AA at 10 mg/mL was used for external calibration. For direct introduction MALDI-FTICR MS measurements, laser shots value was fixed to 200 for all matrices while laser power was optimized in order to reach a 10% ionization threshold. Laser power was set as follow: in positive mode for DHB at 20, for α-CHCA and DCTB at 14 and for ScA at 28. In negative mode for DCTB at 11, for DAN at 14 and for 9AA at 26. Values of the laser power were set as following for optimization in positive mode: for DHB at 12, 15, 17, 18, 20, 22, 24, 26; for α-CHCA at 8, 9, 10, 12, 13, 14, 15, 18; for ScA at 12, 15, 18, 19, 20, 22, 25, 27, 29, 32, 35, 37; for SA at 12, 15, 18, 19, 20, 22; for DCTB at 6, 7, 8, 9, 10, 12, 15, 16 and in negative mode: for 9AA at 15,

17, 20, 23, 25, 27, 30 and 32; for DAN at 10, 13, 14, 15, 17 and for DCTB at 6, 8, 10, 11, 12, 13 and 15. Curves fitted to sigmoid were obtained through the Boltzmann function on OriginPro 2018 (v. b9.5.0.193). Figure 1S shows the curves obtained for optimization of the laser power and the 10% threshold values for the investigated matrices. Except for source parameters, all other experimental parameters used to perform MALDI-FTICR MS measurements were set as in ESI-FTICR MS. These, together with additional parameters of the MALDI source, can be found in table 2S. Experimental design, parameters for internal calibration, molecular formula attribution and data visualization were performed accordingly to ESI-FTICR MS measurements.

2.6 Sample preparation for salt tolerance evaluation

In order to evaluate the salt tolerance of the two sources coupled with FTICR MS, series of solutions spiked with increasing amount of salts were prepared and injected in the instrument. ¼ diluted Hoagland solution was used for the evaluation as used nutritive solution for plant growth. For ESI-FTICR MS measurements, 100-fold diluted SPE solutions in water/methanol (50/50, v/v) were used, while for evaluation on MALDI-FTICR MS, the SPE solution with the DHB matrix 1:10 +0.1 % FA was the only investigated. Salt solution was added at a percentage of 0.01%, 0.05%, 0.1%, 0.5%, 1%, 5% and 10% on the final volume of the obtained solutions for ESI- and MALDI-FTICR MS. Measurements were performed in the two modes according to the experimental parameters used before and each acquisition was performed on 50 accumulated scans.

2.7 Data analysis for ESI-FTICR MS and MALDI-FTICR MS measurements

Following data acquisition, all data arising from both ESI- and MALDI-FTICR MS measurements were treated on Bruker Compass DataAnalysis software (v. 5.1). Each accumulated mass spectrum was peak picked (S/N 8), then mass calibration was confidently performed using a mass list of *Pisum Sativum* RE metabolites identified through DDA-MS (Table 3S). Standard deviation on *m/z* values determined after internal calibration on a set of 34 points was found to be below 0.100 ppm using a linear fit. Spectra related to samples were subtracted of blanks in Xpose mode with ratio 5 and molecular formula were assigned on the subtracted spectra with the common boundaries: $C_{1–50}$, $H_{1–100}$, $N_{1–8}$, $O_{0–30}$, S_{0-1} and P_{0-1}. Attribution was performed considering M + H protonated forms and M + Na, K, Ca adducts for positive mode, while in negative mode only M – H forms were retained. Molecular formulas were assigned for peaks with relative intensity threshold of 0.2 %, within a *mSigma*

limit of 800 and a tolerance mass error of 0.1 ppm. RDBE limit were set from 0 to 80 and H/C ratio from 0 to 3. Data containing assigned formula were exported and manually handled to avoid molecular formula redundancy (molecular formula arising from protonated and adduct forms). Visualization of van Krevelen and double bond equivalent (DBE) plots were obtained through an in-house script. For ESI- and MALDI-FTICR MS, performance evaluation measurements for both 50 and 200 accumulated spectra were acquired in triplicate. For salt tolerance evaluation with the two sources triplicate analysis were acquired by accumulating 50 spectra. Reduced time for analysis was used to limit major salt contamination of ESI source at high salt concentration.

2.8 **Solvents and reagents**

All solvents and additives used to prepare mobile phases and sample solutions for ESI- and MALDI-FTICR MS measurements were LC-MS grade and they were purchased from Fisher Chemical (Pittsburgh, PA). 2,5 Dihydroxybenzoic acid, 9-aminoacridine and trans-2-[3-(4-tert-Butylphenyl)-2-methyl-2-propenylidene] malononitrile were at 98% purity. 1,5-Naphthalenediamine, sinapinic acid and sinapic acid were at 99% purity. All matrices were purchased from Sigma-Aldrich (Saint Luis, MO, USA). LC-MS grade formic acid used for sample acidification was purchased from Sigma-Aldrich (Saint Luis, MO, USA).

3. Results and discussion

Root exudates were submitted to preliminary DDA-MS and to ESI-FTICR MS analysis. This allowed to perform at first the annotation of major compounds based on the manual dereplication of fragmentation spectra and on the use of annotation tools as GNPS. Secondly, thanks to the van Krevelen diagram the global metabolic profile of *P. sativum* root exudates was obtained, highlighting the main chemical families. Once characterization performed with the two first techniques, sample were therefore subjected to MALDI-FTICR MS. The next paragraphs are dedicated to the description of the results with the different mass spectrometry platforms used for the analysis of RE. A summary of the analysis, annotation and interpretation workflow is showed in Figure 1.

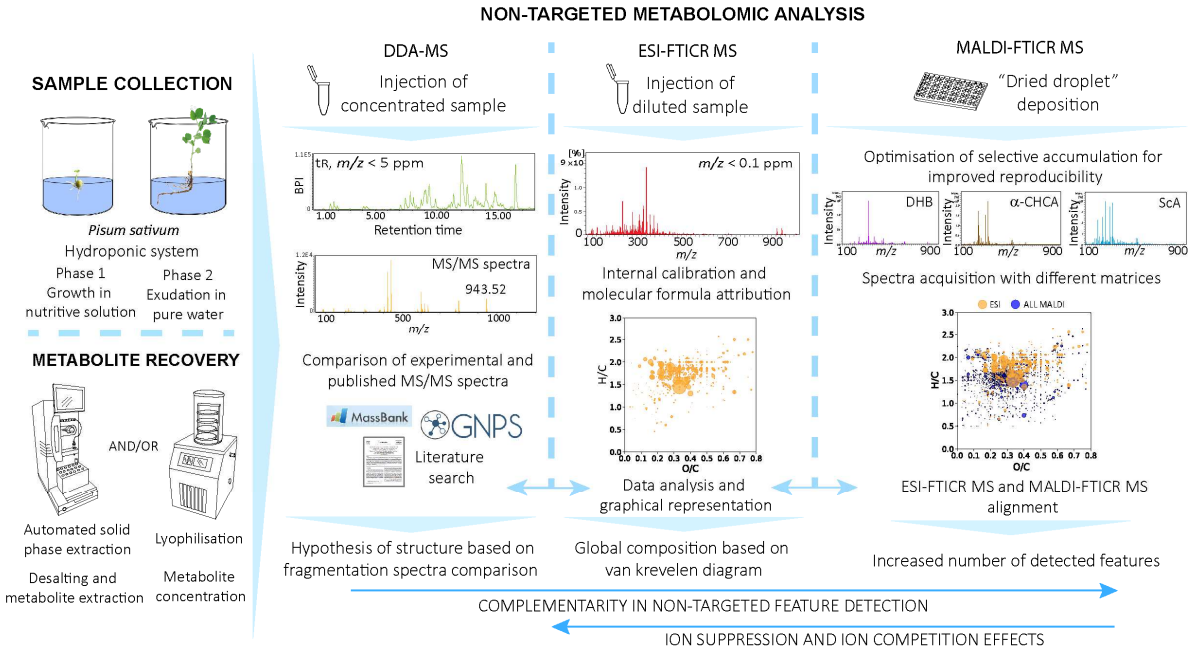

Fig. 1: Workflow used for the non-targeted metabolomic profiling of P. sativum root exudates based on DDA-MS, ESI-FTICR and MALDI-FTICR complementarity

3.1 Identification of *Pisum sativum* root exudates based on DDA-MS measurements and direct introduction ESI-FTICR-MS

At first, DDA-MS measurements on *P. sativum* RE extracts obtained from SPE extraction were performed in ESI positive mode through a hybrid QTOF mass spectrometer. Experimental spectra were then submitted to literature manual search and database match on the GNPS website. A list of metabolites for the 48 major compounds with proposed annotation based on MS/MS spectra can be found in table 3S. The common metabolomic annotation level was used to rank confidences in proposed metabolite structures [89]. The compounds of interest belonged to seven molecular classes, namely nucleosides, amino acids, fatty acids, fatty acid amides, alkaloids, oligopeptides, phosphocholines and triterpenes. In addition to the main compound classes, other minor features presented fragmentation spectra agreeing with polyphenols, glucosyl-phenols and indoles. In this study, on a total of 48, 34 features were annotated at level 2 of confidence and 14 features at a level 3. In fact, some of the most intense metabolites detected via DDA-MS experiments did not found match with literature or database search. For example, feature **19** at *m/z* 367.1863 and molecular formula $C_{18}H_{26}N_2O_6$ was detected together with two analogues and an isomer (features **23**, **25**, **27**) which were separated through chromatography. The fragmentation spectrum (figure 2S) presented two losses of 18 Da with fragment ions at *m/z* 349.17 $[C_{18}H_{24}N_2O_5+H]^+$, *m/z* 331.16

365 $[C_{18}H_{22}N_2O_4+H]^+$, and fragments at lower *m/z* corresponding to *m/z* 139.06 $[C_6H_6N_2O_2+H]^+$,
366 *m/z* 121.04 $[C_6H_4N_2O+H]^+$ and *m/z* 90.05 $[C_5H_4N_2+H]^+$. These metabolites presented a
367 fragmentation pathway similar to that of N-acyl homoserine lactones [90] and they were
368 therefore annotated as fatty acid amides containing histidine or urocanate connected with a
369 C18 or a C16 alkyl chain. Fatty acid amides, as N-acyl homoserine lactones, have been found
370 to have an important role as *quorum sensing* molecules for bacteria communication and
371 cooperation, especially in biofilm formation [91,92]. Moreover, it must be noted that histidine
372 and urocanic acid (a product of histidine metabolism) are found at high concentration in the
373 genus *Fabaceae*, which *P. sativum* belongs to, supporting the proposed annotation made for
374 the fatty acid amides.[93]. Nonetheless, it must be noted that the fragmentation pathway
375 showed some similarities with database spectra of some alkaloids as imidazole [94] or
376 isoquinoline alkaloids [95]. Hence, this alternative annotation should not be excluded.
377 Annotation as fatty acid amides was kept as the most trustable because the analyzed fraction
378 showed the presence of many metabolites connected to lipid and lipid-like molecules. In this
379 regard, our study pointed out on the presence of specialized metabolites, not yet isolated and
380 discovered that can be a starting point for further research. The unambiguous identifications
381 of the proposed metabolites should be performed through comparison of the experimental
382 results with standard compounds or with complementary techniques as isolation and
383 characterization through NMR. For many of the proposed metabolites, the biological role in
384 *P. sativum* root exudation process as not been yet discovered, but according to published
385 literature, *P. sativum* RE contain a high number of nitrogen-containing compounds with basic
386 functional groups that are ionized preferentially in positive mode [96]. In fact, nitrogen
387 compounds have been found to cover an important role in root-bacteria communication and
388 ecosystem functioning. Metabolites for which a hypothesis of structure was formulated (Table
389 3S) were used to create a list of reference compounds to be used as internal mass calibrants in
390 ESI-FTICR MS measurements. Chemical classes were then used to gather the additional
391 features detected through ultra-high-resolution mass spectrometry measurements and to
392 discuss the differences in ionization *via* ESI- and MALDI-FTICR MS (next paragraphs).
393 Once the first information on *P. sativum* RE obtained, 100-fold diluted RE SPE extracts were
394 then submitted to ESI-FTICR MS analysis. Mass spectra of both samples and blanks acquired
395 in positive mode accumulating 200 scans where then internally calibrated using a linear fit.
396 The standard error over a *m/z* 98-1500 range was lower than 0.100 ppm. After blank
397 subtraction, molecular formulas were attributed for one analytical replicate according to the
398 rules described in the materials and methods section. The wide diversity of heteroatoms (N, P,

S) and the presence of many adducts (Na, K and Ca) led often to multiple formula for each peak, especially for high *m/z* values in positive mode. No other adducts (Mg, Mn) resulted in preliminary formula assignment trials and they were therefore not considered. In general, when a double assignment was present, peaks were checked manually to remove unlikely molecular formula. This was performed when possible, based on the highest fit of the isotopic fine structure distributions for proposed formulas and experimental peaks. Conversely, the most logical formula based on the molecular classes that were found through DDA-MS experiments was retained. Nonetheless, it must be considered that different adducts could be present for the same molecule. For this reason, the obtained list was further cleaned up in order to reduce data redundancy and avoid that one molecule ionized in different forms (for example H^+ form and Na^+ form) could led to many different H/C ratios. Hence, molecular formulas of protonated forms were subtracted of a hydrogen and molecular formulas corresponding to Ca adducts were added of a hydrogen. Formula for K and Na adducts were kept unaltered. The list of molecular formula was then used to plot H/C ratios in function of O/C ratios and construct therefore the van Krevelen diagram (figure 3S) for ESI ionization. An in-house Python script was used for data visualization. As expected, an increase of the number of detected features was obtained thanks to ESI-FTICR MS measurements, with 486 molecular formulas assigned in positive mode for the SPE sample. At our best, resulting annotation were submitted to PubChem search in order to propose insight on molecular family and subclasses. Figure 3Sa shows that *P. sativum* RE was characterized by a significant number of nitrogen-containing compounds, which consisted in a wide range of nucleosides and cytokines, amino acids and small oligopeptides, fatty acid amides, alkaloids and phosphocholines. Compounds that did not contain nitrogen or other heteroatoms were confirmed to be the triterpenes soyasaponins, a wide range of fatty acids that includes some plant hormones as jasmonic acid derivates or flavonoids. Among CHO compounds, a group of features that were not detected in DDA-MS had a molecular formula corresponding likely to glycolipids, which was taken as the best annotation. Moreover, thanks to the hypothesis of structures and information on the molecular families present in the sample, some unconventional molecular families were assigned for the first time to a definite zone of the van Krevelen diagram (Figure 3Sb). For example, it was possible to trace back the N-acylethanolamines at H/C =2.0 and O/C = 0.1, the fatty acid amides containing histidine or urocanic acid at H/C = 1.5 and O/C = 0.3 in a zone normally designed for oligopeptides, the soyasaponins glucosides at H/C =1.6 and O/C = 0.4. Similarly, oligopeptides at high N number (N=6 or 7) were placed at H/C = 1.3 and O/C = 0.2 and glycolipids in an intermediate

zone between fatty acids and sugars, at H/C = 2 and O/C = 0.5. The list of metabolites found through ESI-FTICR MS can be found in supplementary material. In general, all molecular formula for the compounds found through DDA-MS were found in their protonated or Na^+, K^+ and Ca^{2+} adducts and were therefore confirmed through ESI-FTICR MS, giving a higher confidence level in metabolites annotation. Despite this, some compounds on a total of 48 annotations were not found in ESI-FTICR MS spectra (table 3S). This could be due to the presence of residual salts or to an important number of ions that led likely to ion suppression and ion competition effects, despite the sample desalting through solid phase extraction. In the attempt to overcome these effects, experiments based on direct introduction MALDI-FTICR MS based on dried droplet deposition were performed and ionization in the two sources compared.

3.2 Optimization of a direct introduction MALDI-FTICR-MS method for a non-targeted metabolomic approach

In ESI measurements samples are commonly injected with a constant flow by direct infusion. This translates likely in constant scan-to-scan ion abundance transmitted to the ICR cell, to reduced error on exact mass measurement and eventually, to good reproducibility of ion intensity in repeated measurements. In contrast, traditional MALDI sample preparation based on the "dried droplet" deposition has as main drawback an inhomogeneous distribution of analytes and matrices crystals in the deposed sample [62]. This represents a problem for quantitative analysis and, in the case of FTICR MS measurements, it can affect the reproducibility due to a change of scan-to-scan ion abundance transmitted to the ICR cell. In order to evaluate ESI and MALDI for a non-targeted metabolomic approach based on FTICR MS, repeatability was evaluated by calculating the relative standard deviation (RSD) on absolute signals intensity within three intra-day acquisitions of 50 accumulated scans for each mass spectrum. Results in ESI-FTICR MS mode obtained for *P. sativum* RE (SPE) samples showed that reproducibility of ion signals for the 85% of the features in the *m/z* range 98-1500 was found appropriate, with deviation typically below 10%. Moreover, most metabolites showed RSD lower than 20% (Figure 2a). For the evaluation of reproducibility in intra-day MALDI-FTICR MS measurements on dried droplet deposed samples for non-targeted metabolomics, 50 scans accumulated spectra were first recorded without any supervision on the scan-to-scan ion abundance transmitted to the ICR cell during acquisition. Figure 2b shows the obtained RSD for MALDI features in unsupervised measurements: only 20% of the

features were found to have a 10% RSD and 77% below the 20%, while RSD up to 60% characterized a greater number of features. In order to minimize the variation of ion abundance in the ICR cell during the acquisition and to improve reproducibility in repeated measurements, an optimization of the selective accumulation was performed. 50 scans accumulated spectra were recorded using different ranges of selective accumulation. Selective accumulation allows to set a minimum (min) and a maximum (max) of intensity [97]. Mass spectra out of this range are discarded from the final average mass spectrum. Three ranges of selective accumulation were tested. A first range with min intensity 5×10^7 and max 5×10^8, a second range at min 1×10^8 and max 5×10^8 and a third range at min 1×10^8 and max 3×10^8. Figure 4S shows the profiles of accumulation on the total acquisition obtained from scan-to-scan total ion current entering in the ICR cell and considered for final spectrum, during a total of 50 scans. In general, more the range of selective accumulation was narrow, more the total ion current resulting from accumulation assumed a linear trend, reducing progressively the "wavy trends" corresponding to low signal accumulation scans, as showed in figures 4Sb and 4Sc. Figure 4Sd shows that an ideal linear trend was obtained when selective accumulation spanned from a min of 1×10^8 to a max of 3×10^8 for each accumulated scan. It is worth to note that the lower limit influenced the signal threshold and its optimization allowed to discard acquisition scans corresponding to low density zone on the MALDI spot in which only signals of the noise were present. In this regard min value at 5×10^7 led to the accumulation of spectra in which no signal corresponding to metabolites were present. While, the value of min selective accumulation equal set to 1×10^8 allowed to obtain total ion signal in the mass spectra in the 9×10^6 – 1×10^7 range. Similarly, the optimization of the max limit avoided accumulation of too many ions in "hot spots". It is worth to note that the overall scan-to-scan intensity with optimized ranges corresponded to an effective min intensity of 1×10^7 to a max effective intensity of 3×10^8 in mass spectra. This range corresponded to the intensity variation in one ESI mass spectrum, allowing a better comparison of final spectra acquired with the two ion sources. The optimization of the selective accumulation range resulted in the overall increase of mass spectra reproducibility and in a higher mass precision. In fact, RSD with MALDI reached satisfying values approaching results obtained with ESI. Figure 2c shows that with optimized ranges, 52% of metabolites had RSD below 10% and 93% in the 20% limit. Similarly, the standard error over a *m/z* 98-1500 range was reduced from 0.150 ppm in the unsupervised analysis to 0.080 ppm using the optimized selective accumulation ranges These results represented an improvement towards a reliable analytical method based on classical deposition method for MALDI-FTICR MS applied to metabolomic analysis,

especially for the confident formula assignment in presence of high atomic diversity Nonetheless, it must be noted that, several scans were discarded yielding to an increase of analysis time up to 150%. For instance, for 200 accumulated scans, the run time was around 5 min with unsupervised analysis and up to 12 to 15 min with the optimized selective accumulation range. Optimization was performed on a same spot containing DHB mix with the sample in proportion 1:10 + 0.1% FA. The laser power was optimized for all matrices in order to get comparable ionization thresholds, the optimized range of selective accumulation fitted with all other conditions.

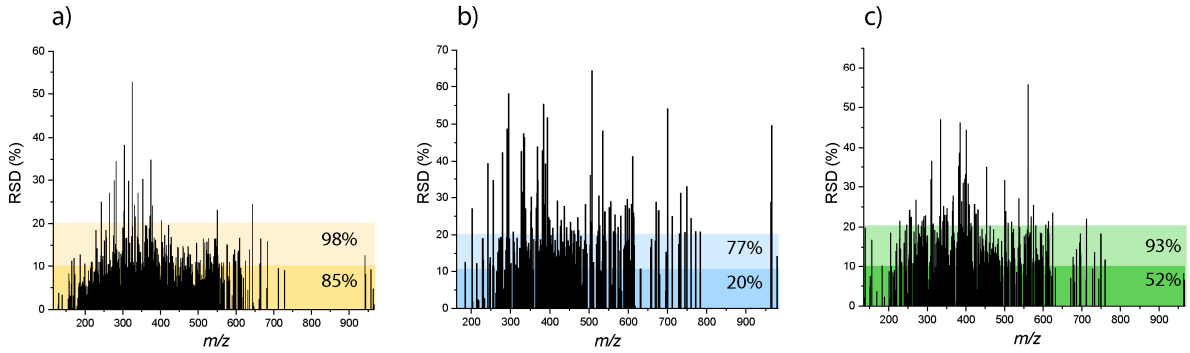

Fig. 2: Relative standard deviation of signal intensity calculated for common metabolites on n=3 replicates found in Pisum Sativum RE for a) direct introduction ESI-FTICR MS, b) MALDI-FTICR MS without optimization of the selective accumulation and c) MALDI-FTICR MS under optimized conditions laying in a selective accumulation range of min=1×10^8 and *max*=3×10^8.

3.3 Evaluation of the efficiency of different MALDI matrices

In order to perform MALDI-FTICR MS analysis in best conditions for non-targeted metabolomic aims, an optimization of the most suited sample/matrix combination was performed. *P. sativum* RE SPE samples were mixed with the 6 matrices selected in this study at a ratio 1:1, 2:1 and 1:10. As ESI-FTICR MS measurements in positive mode were performed on acidified solutions to favor protonated forms against Na^+ and K^+ adducts, the three sample/matrix ratio for each matrix were also tested with the addition of 0.1% FA. For negative mode, the mixtures sample/matrix were used without any further addition. Solutions were deposed using the "dried droplet" method, dried under vacuum and analyzed through MALDI-FTICR MS. Mass spectra for the 24 conditions in positive mode and nine conditions in negative mode were acquired using the optimized selective accumulation range for 50

accumulated scans. Mass spectra were treated as previously described based on the three-steps procedure including internal calibration, blank subtraction and molecular formula assignment. The optimization of the best condition for each matrix was performed at an early stage of the study, the criteria for best condition selection was fixed to the higher number of common *m/z* values found in ESI- and MALDI-FTICR MS spectra and on the highest number of features obtained in order to catch the maximum of detected features for a non-targeted metabolomic study (Figure 3). As alignment based on *m/z* values is performed before molecular formula assignment, isotopic peaks were counted in the total number of peaks. Nonetheless, comparative analysis for the different conditions could be still indicative of the best matrix conditions. For instance, among the six conditions tested for DHB, the ratio sample:matrix 1:10 with the addition of 0.1% FA led to 626 common peaks with ESI-FTICR MS spectra and to a higher number of detected *m/z* values, while the other ratios using DHB were characterized by lower numbers. This led finally to select for further MALDI non-targeted metabolomic investigations in positive mode, the DHB matrix the ratio 1:10 + 0.1% FA, for α-CHCA the ratio 2:1 + 0.1% FA, for ScA and DCTB the ratio 1:1 + 0.1% FA. Moreover, an inspection of the histograms highlighted the presence of a relatively high number of peaks which were exclusively detected in MALDI spectra. These additional molecular formulas could arise both from the presence of multiple adducts formed and/or to additional metabolites for which detection was preferred in MALDI-FTICR MS mode (discussion in the next paragraph). Based on the number of common peaks, the global ionization of the sample in MALDI-FTICR MS was obtained in the order DHB > α-CHCA > ScA > DCTB in positive mode. In fact, the ratio of common peaks on the total *m/z* detected in ESI-FTICR MS spectra (4231) was respectively 14.7%, 11.3%, 6.9% and 5%. Nonetheless, it must be considered that in presence of residual salts especially in ESI, the total *m/z* detected do not correspond necessarily to a corresponding number of unique features and that one compound may be present in form of multiple adducts.

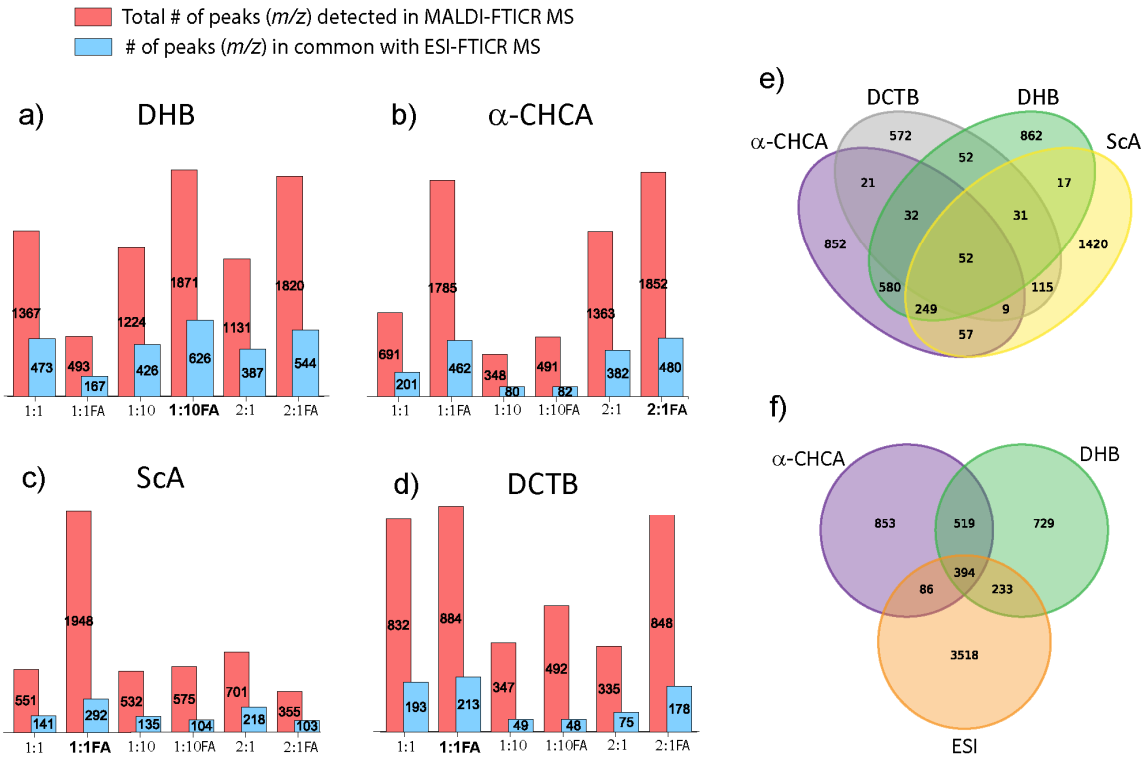

Fig. 3. Evaluation of the total number of peaks and the common peaks found in common with ESI-FTICR MS spectra at different ratio sample/matrix for a) DHB, b) α-CHCA, c) ScA and d) DCTB in MALDI-FTICR MS spectra acquired in positive mode. Best ratios are highlighted in bold style. Venn diagram obtained from alignment of m/z lists for the four selected conditions (DHB 1:10 + 0.1% FA, α-CHCA 2:1 + 0.1% FA, ScA and DCTB 1:1 + 0.1% FA) and for the two highest ranked matrices (DHB 1:10 + 0.1% FA, α-CHCA 2:1 + 0.1% FA) with ESI-FTICR MS spectra are showed respectively in e) and f).

This can explain the surprising low percentage found for common peaks in ESI- and MALDI-FTICR MS spectra at this stage. A discussion on the number of common features obtained for ESI and MALDI after molecular formula assignment is presented in the following paragraphs. In general, a great conformity was found for all tested matrices, as the Venn diagram obtained from alignment of the four best conditions showed the presence of many common *m/z* values, even when two matrices of different chemical nature were compared. Only ScA was characterized by a high number of additional peaks (1420) respect to ESI which were not either in common with other matrices used in MALDI (Figure 3e). Nonetheless, DHB and α-CHCA obtained the highest score when compared with ESI and between the two, DHB seemed to be the most appropriate for non-targeted metabolomics applications. It must be

noted that these results considered only the number of common peaks but did not take into account any information on the type of metabolites, on their intensity or on their detection in form of different adducts. All these concepts will be developed more in the following paragraphs.

MALDI in negative mode resulted in poor metabolites detection (Figure 5S) and low number of common features with ESI spectra (Figure 6S) in respect to positive mode (Figure 3). In fact, alignment in negative mode should be more indicative, as compounds were detected in ESI spectra preferentially as deprotonated forms, removing data redundancy experienced in positive mode. The best ratios sample / matrix were for 9AA 1:1, for DAN 2:1 and for DCTB 1:1. In these conditions, the ratio of common peaks on the total of total *m/z* detected in ESI in negative mode (1987) was 5.2% for 9AA, 6% for DAN and 4.3% for DCTB. In conclusion, spectra in ESI negative mode were very informative and easy to study thanks to the absence of adducts. In comparison, MALDI negative mode did not bring substantial further information in the case of RE of *P. Sativum*. As a contrary, results in MALDI positive mode were highly complementary to the results in ESI positive mode. As a consequence, the negative mode in MALDI was not further investigated in this study and the following discussion will be focused on the non-targeted metabolomic approach in positive ion mode. Nonetheless, MALDI FTICR MS in negative mode should not be discarded *a priori* and further studies could be carried out with other matrices.

3.4 Comparison of ESI-FTICR MS and MALDI-FTICR MS for non-targeted metabolomics on *Pisum sativum* root exudates

Once best conditions for MALDI ionization parameters and best ratios sample/matrix obtained, experiments were repeated for the selected conditions accumulating a higher number of spectra (200 accumulated scans). Measurements performed in triplicates were obtained from three different spots for each condition. Selected conditions for MALDI non-targeted metabolomics on *P. sativum* RE were for DHB analyte/matrix ratio of 1:10 and 0.1% FA, for α-CHCA analyte/matrix ratio of 2:1 and 0.1% FA, for ScA analyte/matrix ratio of 1:1 with 0.1% FA. Comparison was possible with ESI spectra as, scan-to-scan accumulation, total number of scans and final intensity resulted comparable (Figure 4S). Internal calibration, blank subtraction and molecular formula attribution were performed as previously stated.

Figure 7S shows a comparison of the absolute intensity of selected features in ESI and MALDI with the three different matrices. The ionization efficiency towards six main families

were then compared. The six families were nucleosides (Figure 7Sa), amino acids and oligopeptides (7Sb), phosphocholines and phosphoserines (7Sc), fatty acids (7Sd), fatty acid amides containing histidine (7Se) and terpenes (7Sf). For each family, a number ranging from six to nine metabolites were selected according to the presence of a hypothesis of structure raising from DDA-MS measurements or, for assimilation to a chemical family, according to the molecular formula obtained from the ESI measurements. Error bars are relative standard deviation on the three replicates intensities obtained from three different spots. An analysis of the different chemical families allowed to retrieve the presence of particular ionization trends. For example, for all the studied nucleotides (Figure 7Sa), a better ionization yield was obtained in MALDI using α-CHCA as matrix, with an increase of absolute intensity up to 250% respect to the trace obtained in ESI. Conversely, DHB and ScA resulted less efficient in the ionization of nucleosides, leading to lower absolute intensities for the studied metabolites, when compared to ESI. For amino acids and oligopeptides (Figure 7Sb), the number of nitrogen atoms (N) in the molecule resulted crucial in the intensity yield. In fact, for low N number as for phenylalanine (Figure 7S-1b) or for oligopeptide with $N \leq 4$ (Figure 7S-2b, -3b, -4b) ESI resulted in higher signal intensities, while MALDI with DHB matrix enabled a very efficient detection of features containing $N \geq 5$. Moreover, α-CHCA led to higher absolute intensity for oligopeptides containing four to five N. In general, DHB was found to be the most suited matrix for oligopeptides with a signal increase respect to ESI up to 116 % and 85 % respect to α-CHCA. Fatty acids were preferentially ionized and detected in ESI (Figure 7Sd). All fatty acids features were detected in MALDI, but at relatively low intensity. Triterpenes analyzed in the measurements included compounds as soyasaponin di-glucosides. Soyasaponins (Figure 7Sf) showed good ionization yield in MALDI with DHB matrix and in less extent also with α-CHCA. Though, it must be noted that in ESI soyasaponins were ionized as protonated and Na adducts at comparable extent, while in MALDI, even with the addition of a 0.1% FA in the sample/matrix solution, the only adducts were the Na forms. Figure 7Sf shows therefore a comparison of intensity for Na adducts formed in the two sources. In the case of phosphocholines and phosphoserines (Figure 7Sc) and of fatty acid amides containing histidine (Figure 7Se), it was not possible to retrieve a global trend of ionization. For these chemical classes, preferential ionization seemed to be strongly dependent on the peculiar chemical structure. MALDI spectra obtained using ScA showed a preference for the ionization of oligopeptides, alkaloids and for some phosphocholines, but in general,

signals remained of poor intensity and showed therefore no major interest in non-targeted metabolomic approaches.

In general, independently from the matrix, ionization in MALDI appeared to be preferred for molecules containing high number of nitrogen atoms and to increase with the presence of conjugate systems, as in the case of nucleotides. This hypothesis was first been made thanks to rationalization of ionization yield for the metabolites annotated through DDA-MS measurements. In order to deeply investigate this aspect, after molecular formula assignment, the number of features (#) containing N atoms spanning from zero to eight was counted for ESI and for MALDI with DHB, α-CHCA and ScA and plotted as histogram (Figure 4a).

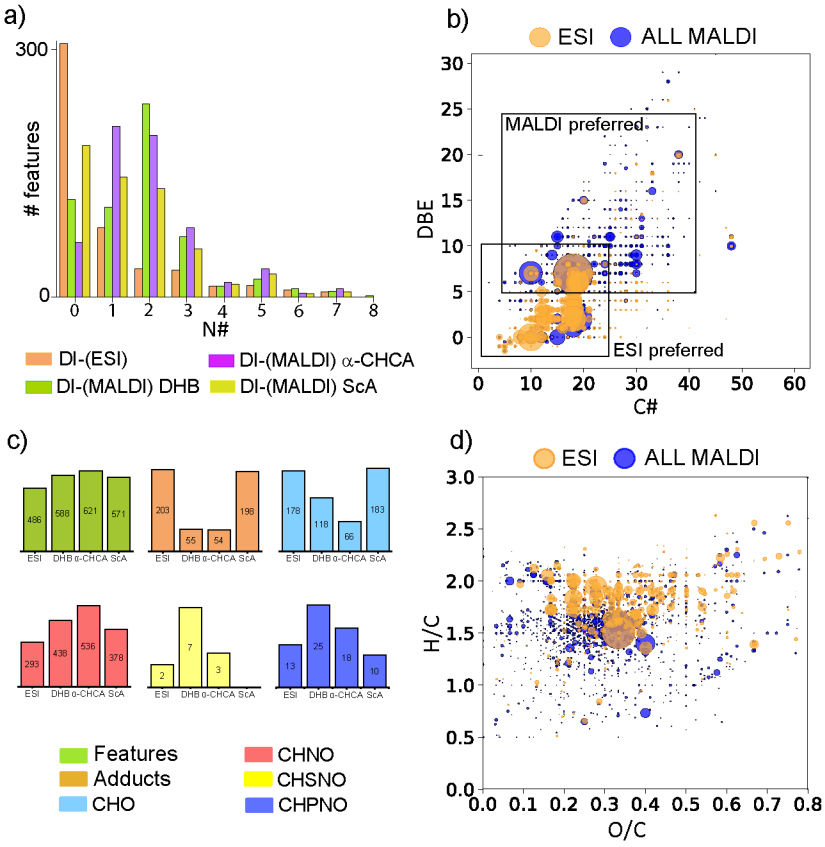

Fig. 4: a) Histograms showing the number of detected features containing from one to eight atoms of nitrogen in ESI (orange), MALDI DHB (green), MALDI a-CHCA (purple) and MALDI ScA (yellow); b) and d) show respectively the DBE vs #C plot and the van Krevelen diagram obtained from molecular formula assignment of ESI (orange) and MALDI (blue) obtained from the three matrices (DHB, a-CHCA and ScA) spectra; c) total number of assigned molecular formulas (green) and adducts (orange) together with the distribution of

features containing CHO (light blue), CHNO (red), CHNSO (yellow) and CHNPO (blue) atoms.

The molecular formula assignment revealed that effectively an increase of the number of features containing N was obtained with MALDI even if intensity for low number of N atoms resulted lower than in ESI, as previously stated (Figure 7S). On the other side, number of oxygen atoms (O#) seemed to have less effects on ionization *via* MALDI (Figure 8S), and a more relevant increase of features containing O# from two to four could be experienced probably as mirror of a higher N# in the molecules. These results agreed with the trends of relative intensity (%) at different N# and O#, for which histograms are showed in figure 9Sa and 9Sb, respectively.

Moreover, the double bond equivalent (DBE) and the carbon number (C#) were calculated from each assigned molecular formula for both ESI and MALDI, gathering together all features obtained from the three matrices (all MALDI). The resulting plot in Figure 4b shows that effectively, additional features detected for the first time through MALDI were generally characterized by higher DBE, up to 25, which corresponded to oligopeptides with N from six to eight. This highlighted that, ionization for unsaturated and high N# molecules was preferred in MALDI while ESI resulted in the preferential ionization of lower DBE compounds. The presence of additional features appeared surprising because MALDI spectra were characterized by simpler profiles respect to ESI spectra, while the obtained van Krevelen diagram showed great similarity (Figure 5).

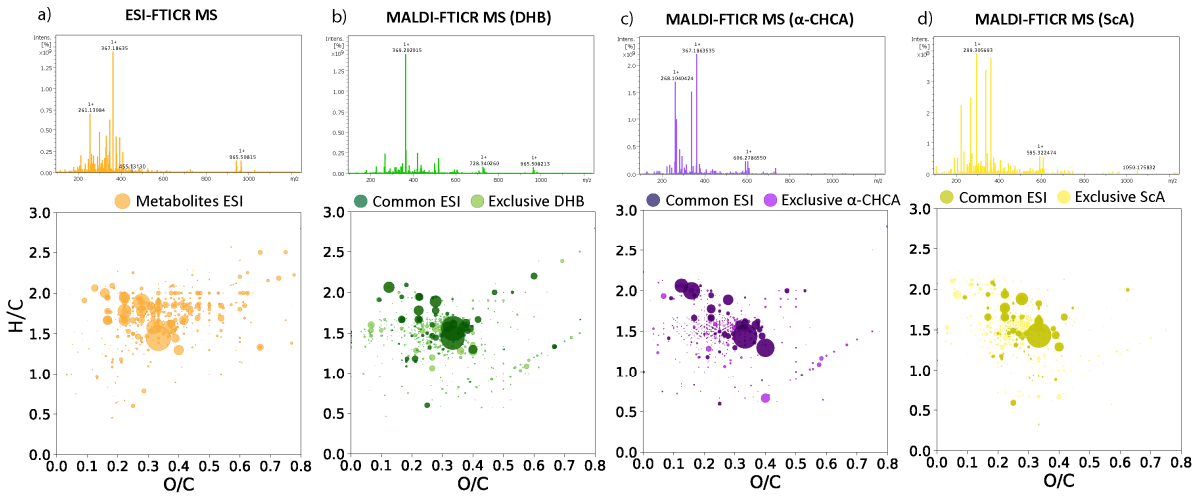

Fig. 5: Mass spectra obtained in positive mode and related van Krevelen diagrams for Pisum sativum root exudates obtained from molecular formula assignment based on ultra-high-

resolution a) ESI-FTICR MS and MALDI-FTICR MS with b) DHB, 2,5-dihydroxybenzoic acid, c) α-CHCA, α-Cyano-4-hydroxycinnamic acid and d) ScA, Sinapinic acid for the SPE desalted P. sativum RE sample.

This mirrored both low signals for some metabolites and both a lower number of Na^+, K^+ and Ca^{2+} adducts. In fact, after molecular formula attribution, most of the features found in MALDI corresponded to protonated forms, while adducts were much less represented (Figure 4c). As an example, feature **35** at *m/z* 211.1325, corresponding to molecular formula $C_{12}H_{18}O_3$ (Table 3S) and annotated *via* DDA-MS as the plant hormone jasmonic acid (annotation level 2), was detected in ESI as Na^+, K^+ and Ca^{2+} adducts, while in MALDI only the protonated form was found. Together with additional features, spectra obtained with MALDI showed common metabolites with ESI. Nonetheless, because of wide differences in ionization, it was difficult to evaluate the correct number of metabolites successfully ionized in both sources (as protonated or adducts) and, counting only the protonated forms, for all matrices around 10% of features were found to be in common. A list of metabolites found in ESI, MALDI (DHB) and MALDI (α-CHCA) can be found as supplementary material. Examples of additional features corresponding to potential metabolites which were detected for the first time in *P. sativum* RE thanks to MALDI were features at *m/z* 152.056675 ($C_5H_5N_5O$, proposed identification guanine), *m/z* 156.076770 ($C_6H_9N_3O_2$ proposed identification histidine), *m/z* 166.072361 ($C_6H_7N_5O$ proposed identification methylguanine). The increase in the number of metabolites detected in MALDI corresponded to small metabolites, but also to molecules with higher *m/z* that are consistent to triterpenes and oligonucleotides as features at *m/z* 328.284593 ($C_{19}H_{37}NO_3$, proposed identification palmitoyl alanine), *m/z* 455.351968 ($C_{30}H_{46}O_3$, proposed identification moronic acid) or *m/z* 740.340207 ($C_{39}H_{45}N_7O_3$, proposed identification cyclo[His-Tyr-Tyr-Leu-Tyr]). Features that were exclusively detected in MALDI are highlighted in bold style in supplementary materials.

Figure 4d shows the van Krevelen diagram obtained from molecular formulas obtained using ESI and MALDI with all matrices. It is worth to note that additional features are not likely to come from MALDI in-source fragmentation as the laser power and the number of shots were optimized for each matrix/sample mixture in order to be just slightly above the matrix ionization threshold. Moreover, the presence of the same additional metabolites in the spectra obtained from two distinct matrices represents an additional proof of the selective detection in MALDI mode. Nonetheless, it should be considered that in non-targeted metabolomic, the different nature of the metabolites could lead to different behaviors of chemical classes in

presence of the matrix, and a complete absence of fragmentation cannot be excluded *a priori* without further investigation. Anyway, results obtained herein shows that MALDI enabled a wide detection of compounds of different chemical classes, and it confirmed its potential as a complementary technique to ESI for a non-targeted metabolomic approach on biological samples.

3.5 Salt tolerance and matrix effects in ESI and MALDI

In order to evaluate salt tolerance of ESI and MALDI techniques for non-targeted metabolomics, mass spectra were recorded for a series of *P. sativum* RE SPE solutions which were spiked with various salt amounts. Indeed, in order to simulate the release of salts in hydroponic cultures, solutions were spiked with aliquots of Hoagland solution [98]. The last is a mixture of many salts for which the concentration is normally expressed in terms of electrical conductivity (EC, dS m^{-1}), which depend on the metal content [99]. For example, ½ Hoagland solution has EC of ~1.1 dS m^{-1}, which for scale comprehension, corresponds to a concentration of ~ 10 mM NaCl, at pH=7 [100]. It is worth to note that, during the collection of the sample, a part of salts can be released together with the metabolites, but at any extent, the concentration should exceed the initial Hoagland EC used for plant growth. Series of solutions for measurements in the two sources were therefore prepared by adding a ¼ Hoagland solution at 0.01%, 0.05%, 0.1%, 0.5%, 1%, 5% and 10% on the final sample. Salt ranges were chosen starting from a minimum equivalent salinity ~ 6 µM NaCl up to ~ 0.6 mM NaCl corresponding to the addition of 10% ¼ Hoagland solution. Measurements were performed in triplicates both for ESI and MALDI. For MALDI, the DHB matrix was selected because of its suitability for non-targeted metabolomic study as demonstrated before. In fact, even if α-CHCA led to higher intensity for many metabolites, DHB resulted in the simultaneous detection of many chemical classes. The variation of the absolute intensity of four case compounds belonging to different chemical classes, namely fatty acids, oligopeptides, soyasaponin triterpenes and nucleosides, at increasing salt concentrations is shown in Figure 6a for ESI and Figure 6b for MALDI.

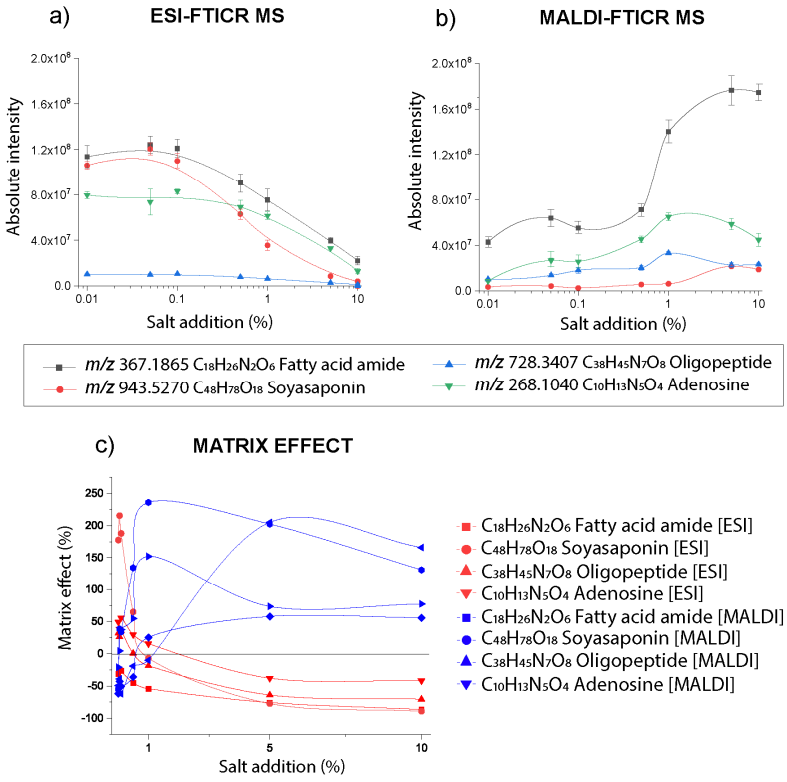

Fig. 6: Variation of the absolute intensity of four compounds of interest at increasing salt concentrations in a) ESI and b) MALDI. Salt concentration is expressed in terms of % of the Hoagland solution volume added to the sample (at log_{10} scale). Matrix effect expressed as $[(I_{ME}/I_{SPE})/I_{SPE}\times100]$ in function of the salt addition for the four case metabolites in ESI and MALDI are showed in panel c. Error bars calculated as standard deviation on three repeated measurements are also shown.

The protonated form for *m/z* 367.1865 $C_{18}H_{26}N_2O_6$ (annotated as fatty acid amide containing urocanate), *m/z* 728.3407 $C_{38}H_{45}N_7O_8$ (annotated as an oligopeptide), *m/z* 268.1040 $C_{10}H_{13}N_5O_4$ (annotated as adenosine) and the sodium adduct for feature at *m/z* 943.5270 $C_{48}H_{78}O_{18}$ (annotated as soyasaponin) were chosen for comparison of the two sources. Two distinct trends were observed in the two sources with the increase of salt concentration. In fact, while in ESI a ~ 6-fold signal drop was measured at salinity 10% for all compounds (Figure 6a), the opposite trend was obtained in MALDI (Figure 6b). Not only the intensity yield for all the ions remained mainly constant up to 0.5% Hoagland, but surprisingly, salts addition had a positive matrix effect on ionization in the range 0.5%-5% leading to a significant increase of the absolute intensity for all ions. Nonetheless, at Hoagland concentration higher than 5%, salt tolerance in MALDI was the optimum while at higher values the ion intensity decreased.

Nevertheless, the mere comparison of the absolute intensity for the case metabolites in the two sources can give only an idea on matrix effects at increasing salinity. For this reason, matrix effects in each source separately were further assessed by comparison of the peak intensity for the studied compounds in the spiked samples and in the starting SPE desalted sample which was used for salt tolerance. Matrix effect was then calculated according to Stahnke et al. [101] as:

$$Matrix\ effect\ (\%) = \frac{I_{ME} - I_{SPE}}{I_{SPE}} \times 100$$

I_{ME} is the intensity of a metabolite in the desalted SPE sample spiked with increasing salt amounts and I_{SPE} is the intensity of the same metabolite in the desalted SPE sample (with any addition of salts). The intensities were retrieved from the mass spectra obtained in ESI and MALDI for both desalted samples and spiked samples. In fact, assessment of matrix effects is usually performed using an analytical standard of known concentration analyzed in the same conditions. However, as concentration of the investigated compounds was not known in this study, the starting solution obtained through SPE before spiking was considered as a standard. It must be noted that this constituted an idealization as ion charge effects due to the sample complexity could influence as well the ionization of compounds in the SPE sample. Nonetheless, as the same SPE sample was used for spiking, the same complexity was kept into account when comparing spectra obtained with the same source. With the proposed formula, matrix effect values higher than 0 % described an increase of the signal in the spiked samples respect to the desalted sample, and therefore they were interpreted as signal enhancement. Similarly, values lower than 0 % denotated signal suppression. Figure 6c shows the obtained matrix effect (%) for four metabolites belonging to the different chemical classes in the two sources at increasing salinity. Signal suppression of around 50 % were obtained in ESI when passing from 0.01 to 1% salt concentration and at maximum salinity (10 % salts) matrix effect accounted to 70-80%. Contrarily, strong signal enhancements were obtained in MALDI with matrix effects accounting up to +150%. This mean that salt concentration equal to a 5% of the total sample volume would triple signal intensity for selected ions. Effectively, as signal enhancement obtained in MALDI resulted to be higher than signal suppression in ESI, it could be likely that for a same compound, a significative overtake of S/N in MALDI respect to ESI was experienced. It is worth to note that matrix effect does not affect all the compounds at the same extent. For example, in MALDI, metabolites with high N number as *m/z* 728.3407 $C_{38}H_{45}N_7O_8$ and *m/z* 268.1040 $C_{10}H_{13}N_5O_4$ showed an absolute intensity drop already at 1% Hoagland concentration (Figure 6a). Ionization enhancement at high salt

concentration has been already showed in previous studies [102,103]and it has been explained as the result of the fast precipitation of salt crystals during evaporation respect to matrix-sample co-crystallization, which would decrease their location on the surface and favor their emplacement at the border of the spot. In the case of this study, ionization enhancement could be due to the peculiar nature of the Hoagland solution and the contained metals. In this extent, three different mechanisms can be considered : 1) the presence of a chelator in the Hoagland solution, namely EDTA (Table 1S), which would lead to the chelation of other metals and to their unavailability in forming adducts with the metabolites of the sample [104]; 2) the ionization of DHB matrix ions containing two aromatic carboxylic acid as adducts, which would reduce the ionization of matrix cluster and lead to an increase of solubility in water (contained in the RE sample and in less extent in the matrix solution), and eventually to a better analyte incorporation and homogeneity [105]; or 3) as already studied adducts can competitively binds with anionic analytes, favoring their desorption and reducing chemical noise [106].

Likely, the improvement of the observed S/N for the metabolites in this study could be explained as the combination of the three factors.

3.6 MALDI-FTICR MS applied to a true lyophilized *Pisum sativum* RE sample

The proposed method based on MALDI for non-targeted metabolomic analysis of *P. sativum* RE has been optimized and evaluated on a metabolite fraction obtained through solid phase extraction. This constituted a simplified sample in which, together with metabolite extraction, a reduction of salts was performed. In most cases, solid phase extraction needs to be optimized for each sample and it represents a long and laborious process which is time-consuming. Moreover, together with salt elimination, the loss of the most polar metabolites can be experienced. As RE contain normally a high number of polar metabolites, lyophilization would lead to a less biased description of the real sample composition, at the expense of a higher salt concentration. For this reason, in order to evaluate the performances of the optimized non-targeted metabolomic approach based on MALDI on high salt concentration RE sample, measurements based on MALDI and on ESI were performed on a lyophilized *P. sativum* RE sample. Mass spectra were acquired, under the same experimental conditions previously used. From preliminary analysis, lyophilized samples resulted in a higher number of K^+ and Na^+ adducts, while Ca^{2+} adducts represented sporadic cases. For this reason, Ca^{2+} was not considered in molecular formula assignment. Repeatability evaluated by

aligning the list of *m/z* values extracted at relative intensity threshold higher than 0.2 %, led to values of 80 % match for ESI, 78 % match for a-CHCA, 76 % for DHB in MALDI measurements. Molecular formulas were attributed accordingly to what was done for SPE desalted samples.

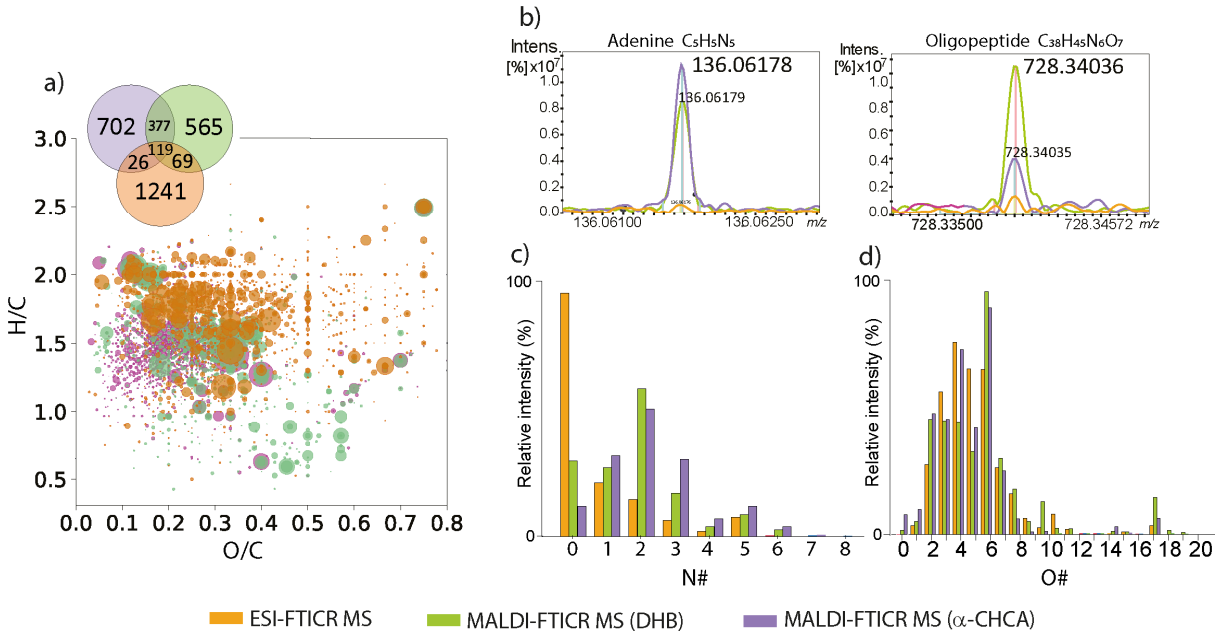

Fig. 7: *a) van Krevelen diagram obtained from formula assignment of ESI (orange), MALDI with DHB (green) and a-CHCA (violet) for P. sativum RE lyophilized samples. b) Overlap of signals traces (ESI, orange; DHB, green; a-CHCA, violet) for two m/z values corresponding to case compounds which were detected only in MALDI. c) Relative intensity of features containing from 1 to 8 atoms of nitrogen in ESI (orange), MALDI DHB (green), MALDI a-CHCA (violet) and MALDI ScA (yellow).*

Figure 7a shows the van Krevelen diagram arising from formula assignment on spectra obtained with the two sources for the lyophilized sample. As expected, a higher number of assigned formulas was globally detected respect to the desalted sample obtained through SPE (Figure 3a), highlighting that desalting led effectively to the loss of part of the metabolites. Among these, a portion of features at O/C higher than 0.5 appeared, highlighting the recovery of a higher proportion of polar metabolites. These molecules could correspond to nucleoside phosphates, cyclic nucleotides, amino acids and glucoside flavonoids. The list of assigned molecular formula for the lyophilized sample in ESI and in MALDI measurements with DHB and a-CHCA can be found as supplementary information. In general, molecular formula assignment confirmed previous results, as a higher number of adducts was assigned in ESI compared to MALDI spectra also for the lyophilized sample (Figure 10Sa).

Figure 7b shows the overlap of relative signal intensity obtained for two case metabolites in the two sources, namely $C_5H_5N_5$ with $[M+H]^+$ at *m/z* 136.06178 annotated as adenine and $C_{38}H_{45}N_6O_7$ with [M+H]+ at *m/z* 728.34036 annotated as an oligopeptide containing proline. While poor intensity signals for the two metabolites characterized ESI spectra, MALDI with both matrices led to higher S/N signals enabling their efficient detection and eventually, confident molecular formula assignment. Effectively, high salinity leading to ion suppression in ESI and ion enhancement in MALDI improved the detection of features in MALDI. This was especially valid for the DHB matrix that showed a strong signal enhancement compared to ESI. These findings agreed with the evolution of ion intensities at the increase of salt concentration presented in the previous paragraph (Figure 6) and allowed also to retrieve the approximative salinity, which was evaluated to be around 2 % (v/v) in lyophilized *P. sativum* RE. At this salt concentration, some metabolites were not detected in ESI but on average a higher number of detected features was obtained compared to MALDI (Figure 7a). Nonetheless, as previously stated, the total number of assigned formulas was redundant in ESI measurements because of the presence of several adducts. The Venn and van Krevelen diagrams were then plotted considering only the protonated forms in ESI and MALDI (Figure 11S). In this case, similar plots were obtained, except for fatty acids and lipids (H/C=1.5-2 and O/C=0.1-0.3), which showed to be the most affected from adduct formation (Figure 10Sb). On the other side, a lower number of formulas only detected in ESI was obtained, keeping the number of common formulas almost unchanged (Figure 10Sb). Trends of relative intensity and number of detected features containing increasing N# and O# (showed respectively in figure 7d, 7d and 11Sa, 11Sb) confirmed results obtained for the SPE desalted sample. The two sources appeared to be highly complementary for a non-targeted metabolomic approach on root exudate samples. MALDI enabled an increase of detected features especially at relatively high salt concentration. Most of the metabolites exclusively detected with MALDI corresponded to nucleosides, alkaloids, flavonoids and highly aromatic compounds such as triterpenes and riboflavin analogues. For example, the exclusive detection in MALDI measurements was experienced for metabolites which molecular formula that could be tentatively assigned to quercetin analogues (*m/z* $C_{15}H_{10}O_7$), lumichrome (*m/z* $C_{12}H_{10}N_4O_2$), lumiflavine (*m/z* $C_{13}H_{12}N_4O_2$), willardine (*m/z* $C_7H_9N_3O_4$) and anhydropisatine (*m/z* $C_{17}H_{12}O_5$). These molecules have a biological importance and they have been found to cover a principal role in *P. sativum* metabolism or to represent important mediators in plant growth and interaction with microorganisms [107–110].

4. Conclusion

In this study, a non-targeted metabolomic approach *via* direct introduction MALDI-FTICR MS based on dried droplet deposition, was optimized on *P. sativum* root exudate samples. Optimized conditions of selective accumulation and best sample:matrix ratio for different matrices enabled improved precision and high metabolite cover up increasing the number of detected unique features compared to ESI-FTICR MS analysis. Moreover, matrix effect evaluation performed on RE spiked with salt showed the presence of ion suppression in ESI-FTICR MS and ion enhancement in MALDI-FTICR MS. Spectra obtained with MALDI were characterized by a lower complexity and led to an increase of detected unique features as a mirror of both lower number of adducts and preferential ionization of compounds at high N# and high DBE. Lyophilized root exudate samples analyzed through the two sources showed a good coverage of metabolite detection and annotation thanks to the ultra-high resolution, mass measure precision and dynamic range of FTICR MS, demonstrating that MALDI could be an alternative and complementary source for non-targeted metabolomics on biological samples. The authors believe that the results of this work are relevant in the field of non-targeted metabolomic and in the analysis of root exudate using a direct introduction approach based on FTICR MS. Moreover, the proposed method *via* direct introduction MALDI FTICR MS based on classic dried droplet deposition could be applied to other type of samples which are affected by matrix effects due to the presence of salts such as DOM and NOM in seawater, humic substances in fresh soil or in other biological samples as algae or blood. However, future works still require addressing some unresolved questions as for example, the optimization of an efficient MALDI FTICR MS method for RE analysis in negative mode or the research of new and more performant matrices for improved metabolite detection, sample homogeneity and high reproducibility for RE analysis. In this extent, solid-ionic or liquid-ionic matrices represent potential candidates for RE analysis through MALDI FTICR MS thanks to their co-crystallization properties and the possibility to be used both in positive and negative mode [111]. Moreover, future investigation should be dedicated also on defining the applicability and the limits of the optimized conditions found in this study on plants belonging to different genus and/or family or to study the RE changes in presence of rhizobacteria in the pursuit of a universal method based on MALDI FTICR MS for a comprehensive RE analysis.

Author contribution: Valentina Calabrese: Conceptualization, Data curation, Formal analysis, Investigation, Methodology, Visualization, Roles/Writing - original draft **Isabelle**

Schmitz-Afonso: Conceptualization, Funding acquisition, Project administration, Resources, Supervision, Validation, Writing - review & editing **Wassila Riah-Anglet:** Methodology, Writing - review & editing **Barbara Pawlak:** Funding acquisition, Project administration, Resources, Writing - review & editing **Isabelle Trinsoutrot -Gattin** Funding acquisition, Project administration, Methodology, Resources **Carlos Afonso:** Conceptualization, Funding acquisition, Project administration, Resources, Supervision, Validation, Writing - review & editing.

Data availability All the data are described within the manuscript. The raw data and metadata analyzed during the current study are available from the corresponding author on request.

Acknowledgments The authors gratefully acknowledge Pascal Cardinael (COBRA, Rouen, France) for the kind provision of the automatic SPE and Benjamin Pionnier (INTERCHIM, France) for support on its utilization. Anne Cauchois (UniLaSalle, Rouen, France) and Carole Burel (CURIB, Rouen, France) for advice in sample collection and sample treatment. Maxime Sueur, Oscar Lacroix-Andrivet and Julien Maillard (COBRA, Rouen, France) for the kind help and provision of the in-house script for FTICR data analysis. All the COBRA team for the support.

Funding This work was partially supported by Normandie Université (NU), the Région Normandie, the Centre National de la Recherche Scientifique (CNRS), Université de Rouen Normandie (URN), INSA Rouen Normandie, Labex SynOrg (ANR-11-LABX-0029), the graduate school for research XL–Chem (ANR-18-EURE-0020 XL CHEM), European Regional Development Fund (ERDF), Innovation Chimie Carnot (I2C) and SFR Normandie Végétal FED 4277. Financial support from Region Normandie and European Union (RIN Recherche Tremplin 2019 BEER) for conducting the research is gratefully acknowledged. Financial support from the IR INFRANALYTICS FR2054 for conducting the research is gratefully acknowledged. This work was supported the European Union's Horizon 2020 Research Infrastructures program (Grant Agreement 731077).

Declaration of competing interest The authors declare that they have no conflict of interest.

References

[1] N. Vinayavekhin, A. Saghatelian, Untargeted metabolomics, Curr. Protoc. Mol. Biol. 90.1 (2010)30 –1 . https://doi.org/10.1002/0471142727.mb3001s90.

[2] A.C. Schrimpe-Rutledge, S.G. Codreanu, S.D. Sherrod, J.A. McLean, Untargeted Metabolomics Strategies—Challenges and Emerging Directions, J. Am. Soc. Mass Spectrom. 27 (2016) 1897–1905. https://doi.org/10.1007/s13361-016-1469-y.

[3] W.B. Dunn, A. Erban, R.J.M. Weber, D.J. Creek, M. Brown, R. Breitling, T. Hankemeier, R. Goodacre, S. Neumann, J. Kopka, M.R. Viant, Mass appeal: Metabolite identification in mass spectrometry-focused untargeted metabolomics, Metabolomics. 9 (2013) 44–66. https://doi.org/ 10.1007/s11306-012-0434-4.

[4] I. Nikolskiy, N.G. Mahieu, Y.J. Chen, R. Tautenhahn, G.J. Patti, An untargeted metabolomic workflow to improve structural characterization of metabolites, Anal. Chem. 85 (2013) 7713–7719. https://doi.org/ 10.1021/ac400751j.

[5] A. Ribbenstedt, H. Ziarrusta, J.P. Benskin, 2018. Development, characterization and comparisons of targeted and non-targeted metabolomics methods, *PLoS One*. 13, e0207082. https://doi.org/10.1371/journal.pone.0207082.

[6] D.C. Sévin, A. Kuehne, N. Zamboni, U. Sauer, Biological insights through nontargeted metabolomics, Curr. Opin. Biotechnol. 34 (2015) 1–8. https://doi.org/10.1016/j.copbio.2014.10.001.

[7] M. Commisso, P. Strazzer, K. Toffali, M. Stocchero, F. Guzzo, 2013. Untargeted metabolomics: An emerging approach to determine the composition of herbal products, Comput. Struct. Biotechnol. J. 4, e201301007. https://doi.org/10.5936/CSBJ.201301007.

[8] C. Hu, J. Shi, S. Quan, B. Cui, S. Kleessen, Z. Nikoloski, T. Tohge, D. Alexander, L. Guo, H. Lin, J. Wang, X. Cui, J. Rao, Q. Luo, X. Zhao, A.R. Fernie, D. Zhang, Metabolic variation between japonica and indica rice cultivars as revealed by non-targeted metabolomics, Sci. Rep. 4 (2014) 1–10. https://doi.org/10.1038/srep05067.

[9] M.F. Turner, A.L. Heuberger, J.S. Kirkwood, C.C. Collins, E.J. Wolfrum, C.D. Broeckling, J.E. Prenni, C.E. Jahn, Non-targeted metabolomics in diverse sorghum breeding lines indicates primary and secondary metabolite profiles are associated with plant biomass accumulation and photosynthesis, Front. Plant Sci. 7 (2016) 953. https://doi.org/10.3389/FPLS.2016.00953.

978 [10] N. Schauer, A.R. Fernie, Plant metabolomics: towards biological function and
979 mechanism, Trends Plant Sci. 11 (2006) 508–516.
980 https://doi.org/10.1016/J.TPLANTS.2006.08.007.

981 [11] F.R. Castro-Moretti, I.N. Gentzel, D. Mackey, A.P. Alonso, Metabolomics as an
982 Emerging Tool for the Study of Plant–Pathogen Interactions, Metabolites, 10 (2020) 52.
983 https://doi.org/10.3390/metabo10020052.

984 [12] V. Vives-Peris, · Carlos De Ollas, · Aurelio Gómez-Cadenas, · Rosa, M. Pérez-
985 Clemente, Root exudates: from plant to rhizosphere and beyond, Plant Cell Rep. 39 (2020) 3–
986 17. https://doi.org/10.1007/s00299-019-02447-5.

987 [13] A. Canarini, C. Kaiser, A. Merchant, A. Richter, W. Wanek, Root exudation of
988 primary metabolites: Mechanisms and their roles in plant responses to environmental stimuli,
989 Front. Plant Sci. 10 (2019) 157. https://doi.org/10.3389/fpls.2019.00157.

990 [14] X. Zhang, R. Diao, X. Zhu, Z. Li, Z. Cai, Metabolic characterization of
991 asthenozoospermia using nontargeted seminal plasma metabolomics, Clin. Chim. Acta. 450
992 (2015) 254–261. https://doi.org/10.1016/J.CCA.2015.09.001.

993 [15] C.V. Carreño-Carrillo, E.V. Sánchez, C.V. Verduzco, J.E. Herbert-Pucheta,
994 Polyphenol-based nuclear magnetic resonance non-targeted metabolomics of temperature-
995 and time-controlled blue and red maize sprouting, SN App. Sci. 3 (2021) 1–10.
996 https://doi.org/10.1007/S42452-021-04171-W.

997 [16] T. Koal, H.-P. Deigner, Challenges in Mass Spectrometry Based Targeted
998 Metabolomics, Curr. Mol. Med. 10.2 (2010) 216–226.
999 https://doi.org/10.2174/156652410790963312

1000 [17] P. Begley, S. Francis-McIntyre, W.B. Dunn, D.I. Broadhurst, A. Halsall, A. Tseng, J.
1001 Knowles, R. Goodacre, D.B. Kell, Development and performance of a gas chromatography-
1002 time-of-flight mass spectrometry analysis for large-scale nontargeted metabolomic studies of
1003 human serum, Anal. Chem.. 81 (2009) 7038–7046. https://doi.org/10.1021/AC9011599.

1004 [18] R. Díaz, H. Gallart-Ayala, J. v. Sancho, O. Nuñez, T. Zamora, C.P.B. Martins, F.
1005 Hernández, S. Hernández-Cassou, J. Saurina, A. Checa, Told through the wine: A liquid
1006 chromatography–mass spectrometry interplatform comparison reveals the influence of the
1007 global approach on the final annotated metabolites in non-targeted metabolomics, J
1008 Chromatogr A. 1433 (2016) 90–97. https://doi.org/10.1016/J.CHROMA.2016.01.010.

[19] V. Calabrese, I. Schmitz-Afonso, C. Prevost, C. Afonso, A. Elomri, Molecular networking and collision cross section prediction for structural isomer and unknown compound identification in plant metabolomics: a case study applied to Zhanthoxylum heitzii extracts, Anal Bioanal Chem. 1 (2022) 3. https://doi.org/10.1007/s00216-022-04059-7.

[20] G.J. Patti, Separation strategies for untargeted metabolomics, J Sep Sci. 34 (2011) 3460–3469. https://doi.org/10.1002/JSSC.201100532.

[21] B. Sarvin, S. Lagziel, N. Sarvin, D. Mukha, P. Kumar, E. Aizenshtein, T. Shlomi, Fast and sensitive flow-injection mass spectrometry metabolomics by analyzing sample-specific ion distributions, Nat Commun. 11 (2020) 1–11. https://doi.org/10.1038/s41467-020-17026-6.

[22] H.A. Haijes, M. Willemsen, M. van der Ham, J. Gerrits, M.L. Pras-Raves, H.C.M.T. Prinsen, P.M. van Hasselt, M.G.M. de Sain-Van der Velden, N.M. Verhoeven-Duif, J.J.M. Jans, Direct Infusion Based Metabolomics Identifies Metabolic Disease in Patients' Dried Blood Spots and Plasma, Metabolites. 9 (2019) 12. https://doi.org/10.3390/metabo9010012.

[23] A. Aharoni, C.H.R. de Vos, H.A. Verhoeven, C.A. Maliepaard, G. Kruppa, R. Bino, D.B. Goodenowe, Nontargeted Metabolome Analysis by Use of Fourier Transform Ion Cyclotron Mass Spectrometry, OMICS, 6 (2002) 217–234.

[24] A.G. Marshall, C.L. Hendrickson, G.S. Jackson, Fourier transform ion cyclotron resonance mass spectrometry: a primer, Mass spectrom rev. 17 (2018) 1–35. https://doi.org/10.1002/(SICI)1098-2787(1998)17:1.

[25] S.C. Brown, G. Kruppa, J.L. Dasseux, Metabolomics applications of FT-ICR mass spectrometry, Mass spectrom rev. 24 (2005) 223–231. https://doi.org/10.1002/MAS.20011.

[26] J. Han, R.M. Danell, J.R. Patel, D.R. Gumerov, C.O. Scarlett, J.P. Speir, C.E. Parker, I. Rusyn, S. Zeisel, C.H. Borchers, Towards high-throughput metabolomics using ultrahigh-field Fourier transform ion cyclotron resonance mass spectrometry, Metabolomics. 4 (2008) 128–140. https://doi.org/10.1007/S11306-008-0104-8.

[27] P.M. Allard, G. Genta-Jouve, J.L. Wolfender, Deep metabolome annotation in natural products research: towards a virtuous cycle in metabolite identification, Curr Opin Chem Biol. 36 (2017) 40–49. https://doi.org/10.1016/J.CBPA.2016.12.022.

[28] C. Roullier-Gall, M. Witting, D. Tziotis, A. Ruf, R.D. Gougeon, P. Schmitt-Kopplin, Integrating analytical resolutions in non-targeted wine metabolomics, Tetrahedron. 71 (2015) 2983–2990. https://doi.org/10.1016/j.tet.2015.02.054.

[29] M. Shahbazy, P. Moradi, G. Ertaylan, A. Zahraei, M. Kompany-Zareh, FTICR mass spectrometry-based multivariate analysis to explore distinctive metabolites and metabolic pathways: A comprehensive bioanalytical strategy toward time-course metabolic profiling of Thymus vulgaris plants responding to drought stress, Plant Sci. 290 (2020) 110257. https://doi.org/10.1016/J.PLANTSCI.2019.110257.

[30] M. Maia, A. Figueiredo, C. Cordeiro, M. Sousa Silva, FT-ICR-MS-based metabolomics: A deep dive into plant metabolism, Mass Spectrom Rev. (2021). https://doi.org/10.1002/MAS.21731.

[31] J.L. Wolfender, J.M. Nuzillard, J.J.J. van der Hooft, J.H. Renault, S. Bertrand, Accelerating Metabolite Identification in Natural Product Research: Toward an Ideal Combination of Liquid Chromatography-High-Resolution Tandem Mass Spectrometry and NMR Profiling, in Silico Databases, and Chemometrics, Anal Chem. 91 (2019) 704–742. https://doi.org/10.1021/acs.analchem.8b05112.

[32] M.B. Comisarow, A.G. Marshall, The Early Development of Fourier Transform Ion Cyclotron Resonance (FT-ICR) Spectroscopy, J Mass Spectrom. 31 (1996) 581–585. https://doi.org/10.1002/(SICI)1096-9888(199606)31:6.

[33] F. Han, Y. Li, X. Zhang, A. Song, J. Zhang, R. Yin, Comparative study of direct injection analysis and liquid chromatography mass spectrometry for identification of chemical constituents in Kudiezi injection by FT-ICR MS, Int J Mass Spectrom. 405 (2016) 32–38. https://doi.org/10.1016/J.IJMS.2016.05.016.

[34] F. Han, Y. Li, X. Zhang, A. Song, H. Zhu, R. Yin, A pilot study of direct infusion analysis by FT-ICR MS for rapid differentiation and authentication of traditional Chinese herbal medicines, Int J Mass Spectrom. 403 (2016) 62–67. https://doi.org/10.1016/J.IJMS.2016.01.012.

[35] M. Gotthardt, B. Kanawati, F. Schmidt, S. Asam, R. Hammerl, O. Frank, T. Hofmann, P. Schmitt-Kopplin, M. Rychlik, Comprehensive Analysis of the Alternaria Mycobolome Using Mass Spectrometry Based Metabolomics, Mol Nutr Food Res. 64 (2020). https://doi.org/10.1002/mnfr.201900558.

[36] B.M. Ruddy, C.L. Hendrickson, R.P. Rodgers, A.G. Marshall, Positive Ion Electrospray Ionization Suppression in Petroleum and Complex Mixtures, Energ Fuel. 32 (2018) 2901–2907. https://doi.org/10.1021/acs.energyfuels.7b03204.

[37] K. Tang, J.S. Page, R.D. Smith, Charge competition and the linear dynamic range of detection in electrospray ionization mass spectrometry, J. Am. Soc. Mass Spectrom. 15 (2004) 1416–1423. https://doi.org/10.1016/J.JASMS.2004.04.034.

[38] A. Furey, M. Moriarty, V. Bane, B. Kinsella, M. Lehane, Ion suppression; A critical review on causes, evaluation, prevention and applications, Talanta. 115 (2013) 104–122. https://doi.org/10.1016/J.TALANTA.2013.03.048.

[39] T.M. Annesley, Ion Suppression in Mass Spectrometry, Clin Chem. 49 (2003) 1041–1044. https://doi.org/10.1373/49.7.1041.

[40] R. Zenobi, R. Knochenmuss, Ion Formation In Maldi Mass Spectrometry, 17 (1999) 337–366. https://doi.org/10.1002/(SICI)1098-2787(1998)17:5.

[41] L.H. Cohen, A.I. Gusev, Small molecule analysis by MALDI mass spectrometry, Anal Bioanal Chem. 373 (2002) 571–586. https://doi.org/10.1007/S00216-002-1321-Z.

[42] K. Strupat, Molecular weight determination of peptides and proteins by ESI and MALDI, Methods Enzymol. 405 (2005) 1–36. https://doi.org/10.1016/S0076-6879(05)05001-9.

[43] M. Levasseur, T. Hebra, N. Elie, V. Guérineau, D. Touboul, V. Eparvier, Classification of Environmental Strains from Order to Genus Levels Using Lipid and Protein MALDI-ToF Fingerprintings and Chemotaxonomic Network Analysis, Microorganisms. 10 (2022) 831. https://doi.org/10.3390/microorganisms10040831.

[44] A.L. Yergey, J.R. Coorssen, P.S. Backlund, P.S. Blank, G.A. Humphrey, J. Zimmerberg, J.M. Campbell, M.L. Vestal, De novo sequencing of peptides using MALDI/TOF-TOF, J. Am. Soc. Mass Spectrom. 13 (2002) 784–791. https://doi.org/10.1016/S1044-0305(02)00393-8.

[45] M. Barthélemy, V. Guérineau, G. Genta-Jouve, M. Roy, J. Chave, R. Guillot, L. Pellissier, J.-L. Wolfender, D. Stien, V. Eparvier, D. Touboul, Identification and dereplication of endophytic Colletotrichum strains by MALDI TOF mass spectrometry and molecular networking, Sci Rep. 10 (2020) 1–16. https://doi.org/10.1038/s41598-020-74852-w.

[46] C. Hao, X. Ma, S. Fang, Z. Liu, S. Liu, F. Song, J. Liu, S.-Y. Liu, Positive-and Negative-ion Matrix-assisted Laser Desorption/Ionization Mass Spectrometry of Saccharides, Rapid Commun. Mass Spectrom. 12 (1998) 345–348. https://doi.org/ 10.1002/rcm.3072.

[47] C. Fenselau, F.A. Demirev, Characterization of intact microorganisms by MALDI mass spectrometry, Mass Spectrom Rev. 20 (2001) 157–171. https://doi.org/10.1002/MAS.10004.

[48] H.Y. Wang, X. Chu, Z.X. Zhao, X.S. He, Y.L. Guo, Analysis of low molecular weight compounds by MALDI-FTICR-MS, J Chromatogr B Analyt Technol Biomed Life Sci. 879 (2011) 1166–1179. https://doi.org/10.1016/J.JCHROMB.2011.03.037.

[49] P. Champy, V. Guérineau, O. Laprévote, molecules MALDI-TOF MS Profiling of Annonaceous Acetogenins in Annona muricata Products for Human Consumption, Molecules. 14 (2009) 5235–5246. https://doi.org/10.3390/molecules14125235.

[50] I.M. Taban, A.F.M. Altelaar, Y.E.M. van der Burgt, L.A. McDonnell, R.M.A. Heeren, J. Fuchser, G. Baykut, Imaging of Peptides in the Rat Brain Using MALDI-FTICR Mass Spectrometry, J Am Soc Mass Spectrom. 18 (2007) 145–151. https://doi.org/10.1016/j.jasms.2006.09.017.

[51] S.S. Dekeyser, K.K. Kutz-Naber, J.J. Schmidt, G.A. Barrett-Wilt, L.J. Li, N.C. Bird, S.J. Atkinson, M.R. Clench, D. Mangnall, A.W. Majeed, M. Stoeckli, D. Staab, A. Schweitzer, Y. Hsieh, R. Casale, E. Fukuda, J.W. Chen, I. Knemeyer, J. Wingate, R. Morrison, W. Korfmacher, J. Chen, W.A. Korfmacher, S. Khatib-Shahidi, M. Andersson, J.L. Herman, T.A. Gillespie, R.M. Caprioli, M.L. Reyzer, L. Signor, E. Varesio, R.F. Staack, V. Starke, W.F. Richter, G. Hopfgartner, K.K. Kutz, L. Li, E.A. Stemmler, C.R. Cashman, D.I. Messinger, N.P. Gardner, P.S. Dickinson, A.E. Christie, MALDI-FTICR Imaging Mass Spectrometry of Drugs and Metabolites in Tissue, Anal Chem. 80 (2008) 5648–5653. https://doi.org/10.1021/AC800617S.

[52] B.A. Boughton, D. Thinagaran, D. Sarabia, A. Bacic, U. Roessner, Mass spectrometry imaging for plant biology: a review, Phytochem Rev. 15 (2016) 445–488. https://doi.org/10.1007/S11101-015-9440-2.

[53] N.A. dos Santos, L.M. de Souza, F.E. Pinto, C.J. de Macrino, C.M. de Almeida, B.B. Merlo, P.R. Filgueiras, R.S. Ortiz, R. Mohana-Borges, W. Romão, LDI and MALDI-FT-ICR

imaging MS in: Cannabis leaves: Optimization and study of spatial distribution of cannabinoids, Anal Methods. 11 (2019) 1757–1764. https://doi.org/10.1039/c9ay00226j.

[54] N.A. dos Santos, C.M. de Almeida, F.F. Gonçalves, R.S. Ortiz, R.M. Kuster, D. Saquetto, W. Romão, Analysis of Erythroxylum coca Leaves by Imaging Mass Spectrometry (MALDI-FT-ICR IMS), J Am Soc Mass Spectrom. 32 (2021) 946–955. https://doi.org/10.1021/jasms.0c00449.

[55] K. Takahashi, T. Kozuka, A. Anegawa, A. Nagatani, T. Mimura, Development and Application of a High-Resolution Imaging Mass Spectrometer for the Study of Plant Tissues, Plant Cell Physiol. 56 (2015) 1329–1338. https://doi.org/10.1093/PCP/PCV083.

[56] D. Veličković, V.S. Lin, A. Rivas, C.R. Anderton, J.J. Moran, An approach for broad molecular imaging of the root-soil interface via indirect matrix-assisted laser desorption/ionization mass spectrometry, Soil Biol Biochem. 146 (2020) 107804. https://doi.org/10.1016/J.SOILBIO.2020.107804.

[57] D. Veličković, R.K. Chu, G.L. Myers, A.H. Ahkami, C.R. Anderton, An approach for visualizing the spatial metabolome of an entire plant root system inspired by the Swiss-rolling technique, J Mass Spectrom. 55 (2020) e4363. https://doi.org/10.1002/JMS.4363.

[58] S.A. Stopka, L.Z. Samarah, J.B. Shaw, A. v. Liyu, D. Veličković, B.J. Agtuca, C. Kukolj, D.W. Koppenaal, G. Stacey, L. Paša-Tolić, C.R. Anderton, A. Vertes, Ambient Metabolic Profiling and Imaging of Biological Samples with Ultrahigh Molecular Resolution Using Laser Ablation Electrospray Ionization 21 Tesla FTICR Mass Spectrometry, Anal Chem. 91 (2019) 5028–5035. https://doi.org/10.1021/acs.analchem.8b05084.

[59] A. Onzo, R. Pascale, M.A. Acquavia, P. Cosma, J. Gubitosa, C. Gaeta, P. Iannece, Y. Tsybin, V. Rizzi, | Antonio Guerrieri, R. Ciriello, G. Bianco, 2021. Untargeted analysis of pure snail slime and snail slime-induced Au nanoparticles metabolome with MALDI FT-ICR MS. J Mass Spectrom. 56 e4722. https://doi.org/10.1002/jms.4722.

[60] A.N. Krutchinsky, B.T. Chait, On the mature of the chemical noise in MALDI mass spectra, J Am Soc Mass Spectrom. (2002) 129–134. https://doi.org/10.1016/S1044-0305(01)00336-1.

[61] C. Pan, S. Xu, H. Zhou, Y. Fu, M. Ye, H. Zou, Recent developments in methods and technology for analysis of biological samples by MALDI-TOF-MS, Anal. Bioanal. Chem. 387 (2007) 193–204. https://doi.org/10.1007/S00216-006-0905-4

[62] M.B. O'Rourke, S.P. Djordjevic, M.P. Padula, The quest for improved reproducibility in MALDI mass spectrometry, Mass Spectrom Rev. 37 (2018) 217–228. https://doi.org/10.1002/MAS.21515.

[63] Y.N. Chai, D.P. Schachtman, Root exudates impact plant performance under abiotic stress, Trends Plant Sci. 27 (2022) 80–91. https://doi.org/10.1016/j.tplants.2021.08.003.

[64] V. Venturi, C. Keel, Signaling in the Rhizosphere, Trends Plant Sci. 21 (2016) 187–198. https://doi.org/10.1016/j.tplants.2016.01.005.

[65] T. Tian, A. Reverdy, Q. She, B. Sun, Y. Chai, The role of rhizodeposits in shaping rhizomicrobiome, Environ Microbiol Rep. 12 (2020) 160–172. https://doi.org/10.1111/1758-2229.12816.

[66] J. Sasse, E. Martinoia, T. Northen, Feed Your Friends: Do Plant Exudates Shape the Root Microbiome?, Trends Plant Sci. 23 (2018) 25–41. https://doi.org/10.1016/j.tplants.2017.09.003.

[67] M.K. Hassan, J.A. McInroy, J.W. Kloepper, The Interactions of Rhizodeposits with Plant Growth-Promoting Rhizobacteria in the Rhizosphere: A Review, Agriculture 142 (2019) 142. https://doi.org/10.3390/AGRICULTURE9070142.

[68] A. Kumar, A. Dubey, Rhizosphere microbiome: Engineering bacterial competitiveness for enhancing crop production, J. Adv. Res. 24 (2020) 337–352. https://doi.org/10.1016/j.jare.2020.04.014.

[69] N.M. van Dam, H.J. Bouwmeester, Metabolomics in the Rhizosphere: Tapping into Belowground Chemical Communication, Trends Plant Sci. 21 (2016) 256–265. https://doi.org/10.1016/j.tplants.2016.01.008.

[70] E. Oburger, D.L. Jones, Sampling root exudates-Mission impossible?, Rhizosphere, 6 (2018) 116–133. https://doi.org/10.1016/j.rhisph.2018.06.004.

[71] M. Escolà Casas, V. Matamoros, Analytical challenges and solutions for performing metabolomic analysis of root exudates, Trends Environ. Anal. Chem. 31 (2021) e00130. https://doi.org/10.1016/J.TEAC.2021.E00130.

[72] V. Vranova, K. Rejsek, K.R. Skene, D. Janous, P. Formanek, Methods of collection of plant root exudates in relation to plant metabolism and purpose: A review, J. Plant. Nutr. Soil Sci. 176 (2013) 175–199. https://doi.org/10.1002/JPLN.201000360.

[73] S. Hosseinzadeh, Y. Verheust, G. Bonarrigo, S. van Hulle, Closed hydroponic systems: operational parameters, root exudates occurrence and related water treatment, Rev. Environ. Sci. Biotechnol. 16 (2017) 59–79. https://doi.org/10.1007/S11157-016-9418-6.

[74] J.E. Son, H.J. Kim, T.I. Ahn, Hydroponic systems, in: Plant Factory: An Indoor Vertical Farming System for Efficient Quality Food Production: Second Edition, Elsevier Inc., 2019, pp. 273–283.

[75] C. Maucieri, C. Nicoletto, R. Junge, Z. Schmautz, P. Sambo, M. Borin, Hydroponic systems and water management in aquaponics: A review, Ital. J. Agron. 13 (2018) 1–11. https://doi.org/10.4081/IJA.2017.1012.

[76] N. Sharma, N. Singh, Hydroponics as an advanced technique for vegetable production: An overview Hydroponic View project Organic Farming View project, J Soil Water Conserv. 17 (2018) 364–371. https://doi.org/10.5958/2455-7145.2018.00056.5.

[77] P. Dundek, L. Holík, T. Rohlík, L. Hromádko, V. Vranová, K. Rejšek, P. Formánek, Methods of plant root exudates analysis: a review, Acta Univ. Agric. Silvic. Mendel. Brun. 59 (2011): 241–6.

[78] Gransee A, Wittenmayer L. "Qualitative and quantitative analysis of water-soluble root exudates in relation to plant species and development." J. Plant. Nutr. Soil Sci. 163 (2000): 381–385.

[79] Y. Tsuno, T. Fujimatsu, K. Endo, A. Sugiyama, K. Yazaki, Soyasaponins: A New Class of Root Exudates in Soybean (Glycine max), Plant Cell Physiol. 59 (2018) 366–375. https://doi.org/10.1093/PCP/PCX192.

[80] A. Evidente, A. Cimmino, M. Ferna Ndez-Aparicio, A. Andolfi, D. Rubiales, A. Motta, Polyphenols, Including the New Peapolyphenols A-C, from Pea Root Exudates Stimulate Orobanche foetida Seed Germination, J. Agric. Food Chem. 58 (2010) 2902–2907. https://doi.org/10.1021/jf904247k.

[81] L.E. Makarova, L. v. Dudareva, I.G. Petrova, G.G. Vasil'eva, Secretion of Phenolic Compounds into Root Exudates of Pea Seedlings upon Inoculation with Rhizobium leguminosarum bv. viceae or Pseudomonas siringae pv. pisi, Appl. Biochem. Microbiol. 52 (2016) 205–209. https://doi.org/10.1134/S0003683816020095.

[82] Y.-H. Kuo, F. Lambein, F. Ikegami, R. van Parijs, Isoxazolin-5-ones and Amino Acids in Root Exudates of Pea and Sweet Pea Seedlings', Plant Physiol. 70 (1982) 1283–1289. https://academic.oup.com/plphys/article/70/5/1283/6078810.

[83] A. Evidente, M. Fernández-Aparicio, A. Cimmino, D. Rubiales, A. Andolfi, A. Motta, Peagol and peagoldione, two new strigolactone-like metabolites isolated from pea root exudates, Tetrahedron Letters. 50 (2009) 6955–6958. https://doi.org/10.1016/j.tetlet.2009.09.142.

[84] K. Yoneyama, X. Xie, H. Sekimoto, Y. Takeuchi, S. Ogasawara, K. Akiyama, H. Hayashi, K. Yoneyama, Strigolactones, host recognition signals for root parasitic plants and arbuscular mycorrhizal fungi, from Fabaceae plants, New Phytol.179 (2008) 484–494. https://doi.org/10.1111/J.1469-8137.2008.02462.X.

[85] E. Foo, N.W. Davies, Strigolactones promote nodulation in pea, Planta, 234 (2011) 1073–1081. https://doi.org/10.1007/s00425-011-1516-7.

[86] K. Giles, J.P. Williams, I. Campuzano, Enhancements in travelling wave ion mobility resolution, Rapid Commun. Mass Spectrom. 25 (2011) 1559–1566. https://doi.org/10.1002/RCM.5013.

[87] J.S. Yu, L.F. Nothias, M. Wang, D.H. Kim, P.C. Dorrestein, K. bin Kang, H.H. Yoo, Tandem Mass Spectrometry Molecular Networking as a Powerful and Efficient Tool for Drug Metabolism Studies, Anal. Chem. 94 (2022) 1456–1464. https://doi.org/10.1021/ACS.ANALCHEM.1C04925.

[88] L.F. Nothias, D. Petras, R. Schmid, K. Dührkop, J. Rainer, A. Sarvepalli, I. Protsyuk, M. Ernst, H. Tsugawa, M. Fleischauer, F. Aicheler, A.A. Aksenov, O. Alka, P.M. Allard, A. Barsch, X. Cachet, A.M. Caraballo-Rodriguez, R.R. da Silva, T. Dang, N. Garg, J.M. Gauglitz, A. Gurevich, G. Isaac, A.K. Jarmusch, Z. Kameník, K. bin Kang, N. Kessler, I. Koester, A. Korf, A. le Gouellec, M. Ludwig, C. Martin H, L.I. McCall, J. McSayles, S.W. Meyer, H. Mohimani, M. Morsy, O. Moyne, S. Neumann, H. Neuweger, N.H. Nguyen, M. Nothias-Esposito, J. Paolini, V. v. Phelan, T. Pluskal, R.A. Quinn, S. Rogers, B. Shrestha, A. Tripathi, J.J.J. van der Hooft, F. Vargas, K.C. Weldon, M. Witting, H. Yang, Z. Zhang, F. Zubeil, O. Kohlbacher, S. Böcker, T. Alexandrov, N. Bandeira, M. Wang, P.C. Dorrestein, Feature-based molecular networking in the GNPS analysis environment, Nat. Methods. 17 (2020) 905–908. https://doi.org/10.1038/s41592-020-0933-6.

[89] L.W. Sumner, A.E. Alexander, A. Ae, D.B. Ae, M.H.B. Ae, R. Beger, C.A. Daykin, A.E. Teresa, W.-M. Fan, A.E. Oliver, F. Ae, R. Goodacre, A.E. Julian, L. Griffin, A.E. Thomas, H. Ae, N. Hardy, A.E. James, H. Ae, R. Higashi, A.E. Joachim, K. Ae, A.N.L. Ae, J.C. Lindon, A.E. Philip, M. Ae, A.W.N. Ae, M.D. Reily, J.J.T. Ae, M.R. Viant, L.W. Sumner, A. Amberg, D. Barrett, M.H. Beale, R. Beger, C.A. Daykin, Á.R. Higashi, R. Higashi, O. Fiehn, R. Goodacre, Proposed minimum reporting standards for chemical analysis Chemical Analysis Working Group (CAWG) Metabolomics Standards Initiative (MSI), Metabolomics. 3 (2007) 211–221. https://doi.org/10.1007/s11306-007-0082-2.

[90] A.M.S. Rodrigues, R. Lami, K. Escoubeyrou, L. Intertaglia, C. Mazurek, M. Doberva, P. Pérez-Ferrer, D. Stien, Straightforward N-Acyl Homoserine Lactone Discovery and Annotation by LC−MS/MS-based Molecular Networking, J. Proteome Res. 21 (2022) 635–642. https://doi.org/10.1021/acs.jproteome.1c00849.

[91] M. Teplitski, J.B. Robinson, W.D. Bauer, Plants secrete substances that mimic bacterial N-acyl homoserine lactone signal activities and affect population density-dependent behaviors in associated bacteria. Mol. Plant Microbe Interact. 13 (2000): 637-648. https://doi.org/10.1094/MPMI.2000.13.6.637

[92] S.C. Kim, K.D. Chapman, E.B. Blancaflor, Fatty acid amide lipid mediators in plants, Plant Sci. 178 (2010) 411–419. https://doi.org/10.1016/j.plantsci.2010.02.017.

[93] C. Vidal-Valverde, J. Frias, A. Hernández, P.J. Martín-Alvarez, I. Sierra, C. Rodríguez, I. Blazquez, G. Vicente, Assessment of nutritional compounds and antinutritional factors in pea (Pisum sativum) seeds, J. Sci. Food Agric. 83 (2003) 298–306. https://doi.org/10.1002/JSFA.1309.

[94] A.C.F. Sawaya, I.N. Abreu, N.L. Andreazza, M.N. Eberlin, P. Mazzafera, HPLC-ESI-MS/MS of Imidazole Alkaloids in Pilocarpus microphyllus, Molecules, 13 (2008) 1518–1529. https://doi.org/10.3390/MOLECULES13071518.

[95] Z. Qing, Y. Xu, L. Yu, J. Liu, X. Huang, Z. Tang, P. Cheng, J. Zeng, Investigation of fragmentation behaviours of isoquinoline alkaloids by mass spectrometry combined with computational chemistry, Sci Rep. 10 (2020) 1–13. https://doi.org/10.1038/s41598-019-57406–7.

[96] N. Sawatsky, R.J. Soper, A quantitative measurement of the nitrogen loss from the root system of field peas (Pisum avense L.) grown in the soil, Soil Biol. Biochem. 23 (1991): 255–259.

[97] J.S. Ramírez-Pradilla, C. Blanco-Tirado, M. Hubert-Roux, P. Giusti, C. Afonso, M.Y. Combariza, Comprehensive Petroporphyrin Identification in Crude Oils Using Highly Selective Electron Transfer Reactions in MALDI-FTICR-MS, Energy Fuels. 33 (2019) 3899–3907. https://doi.org/10.1021/ACS.ENERGYFUELS.8B04325.

[98] C.J. Asher, D.G. Edwards, Modern solution culture techniques, Inorganic plant nutrition. Springer, Berlin, Heidelberg, (1983) 94–119.

[99] U.C. Samarakoon, P.A. Weerasinghe, W.A.P. Weerakkody, Effect of Electrical Conductivity [EC] of the Nutrient Solution on Nutrient Uptake, Growth and Yield of Leaf Lettuce (Lactuca sativa L.) in Stationary Culture, Acta Horticulturae, 1266 (2019) 137–144. https://doi.org/10.17660/ActaHortic.2019.1266.19.

[100] S.H. van Delden, M.J. Nazarideljou, L.F.M. Marcelis, Nutrient solutions for Arabidopsis thaliana: a study on nutrient solution composition in hydroponics systems, Plant Methods. 16 (2020) 1–14. https://doi.org/10.1186/S13007-020-00606-4.

[101] H. Stahnke, S. Kittlaus, nther Kempe, L. Alder, Reduction of Matrix Effects in Liquid Chromatography−Electrospray Ionization−Mass Spectrometry by Dilution of the Sample Extracts: How Much Dilution is Needed?, Anal. Chem. 84 (2011) 1474–1482. https://doi.org/10.1021/ac202661j.

[102] M. Dufresne, N.H. Patterson, J.L. Norris, R.M. Caprioli, Combining Salt Doping and Matrix Sublimation for High Spatial Resolution MALDI Imaging Mass Spectrometry of Neutral Lipids, Anal. Chem. 91 (2019) 12928–12934. https://doi.org/10.1021/ACS.ANALCHEM.9B02974.

[103] S. Xu, M. Ye, D. Xu, X. Li, C. Pan, H. Zou, Matrix with high salt tolerance for the analysis of peptide and protein samples by desorption/ionization time-of-flight mass spectrometry, Anal. Chem. 78 (2006) 2593–2599. https://doi.org/10.1021/AC051572A.

[104] M. Bourdat-Deschamps, S. Leang, N. Bernet, J.J. Daudin, S. Nélieu, Multi-residue analysis of pharmaceuticals in aqueous environmental samples by online solid-phase extraction-ultra-high-performance liquid chromatography-tandem mass spectrometry: Optimisation and matrix effects reduction by quick, easy, cheap, effective, rugged and safe

extraction, J. Chromatogr. A. 1349 (2014) 11–23. https://doi.org/10.1016/j.chroma.2014.05.006.

[105] J.M. Asara, J. Allison, Enhanced Detection of Phosphopeptides in Matrix-Assisted Laser Desorption/Ionization Mass Spectrometry Using Ammonium Salts, J. Am. Soc. Mass Spectrom. 10 (1999) 35–44.

[106] I.P. Smirnov, X. Zhu, T. Taylor, Y. Huang, P. Ross, I.A. Papayanopoulos, S.A. Martin, D.J. Pappin, Suppression of r-Cyano-4-hydroxycinnamic Acid Matrix Clusters and Reduction of Chemical Noise in MALDI-TOF Mass Spectrometry, Anal. Chem. 76 (2004) 2958–2965. https://doi.org/10.1021/ac035331j.

[107] F.D. Dakora, V.N. Matiru, A.S. Kanu, Rhizosphere ecology of lumichrome and riboflavin, two bacterial signal molecules eliciting developmental changes in plants, Front. Plant Sci. 6 (2015) 700. https://doi.org/10.3389/fpls.2015.00700.

[108] F. Lambein, R. van Parijs, Isolation and characterization of 1-alanyl-uracil (willardiine) and 3-alanyl-uracil (ISO-willardiine) from Pisum sativum." Biochem. Biophys. Res. Commun. 32 (1968) 474–479. https://doi.org/10.1016/0006-291X(68)90686-4.

[109] H. Kato-Noguchi, Isolation and identification of an allelopathic substance in Pisum sativum, Phytochemistry, 62 (2003) 1141–1144. https://doi.org/10.1016/S0031-9422(02)00673-8.

[110] S. Steinkellner, V. Lendzemo, I. Langer, P. Schweiger, T. Khaosaad, J.P. Toussaint, H. Vierheilig, Flavonoids and Strigolactones in Root Exudates as Signals in Symbiotic and Pathogenic Plant-Fungus Interactions, Molecules , 12 (2007) 1290. https://doi.org/10.3390/12071290.

[111] Armstrong, D.W., Zhang, L.K., He, L. and Gross, M.L., 2001. Ionic liquids as matrixes for matrix-assisted laser desorption/ionization mass spectrometry. Anal chem, 73 (15) 3679–3686. https://doi.org/10.1021/ac010259f